Chemical Geology 339 (2013) 141–156

Contents lists available at SciVerse ScienceDirect

Chemical Geology

journal homepage: www.elsevier.com/locate/chemgeo

Helium and carbon isotope systematics of cold "mazuku" CO_2 vents and hydrothermal gases and fluids from Rungwe Volcanic Province, southern Tanzania

P.H. Barry [a,*], D.R. Hilton [a], T.P. Fischer [b], J.M. de Moor [b], F. Mangasini [c], C. Ramirez [d]

[a] Fluids and Volatiles Laboaratory, Scripps Institution of Oceanography, UCSD, La Jolla, California 92093-0244, USA
[b] Department of Earth and Planetary Sciences, MSC 03 2040, 1 University of New Mexico, Albuquerque, New Mexico 87131-0001, USA
[c] Department of Mining and Mineral Processing Engineering, University of Dar Es Salaam, PO Box 35131, Dar Es Salaam, Tanzania
[d] Centro de Investigaciones en Ciencias Geologicas, Escuela Centroamericana de Geologia, Universidad de Costa Rica, Costa Rica

ARTICLE INFO

Article history:
Accepted 3 July 2012
Available online 10 July 2012

Keywords:
Helium isotopes
Carbon isotopes
$CO_2/^3He$
Rungwe Volcanic Province
East African Rift
System

ABSTRACT

We report new helium and carbon isotope ($^3He/^4He$ and $\delta^{13}C$) and relative abundance ($CO_2/^3He$) characteristics of a suite of 20 gases and fluids (cold mazuku-like CO_2 vents, bubbling mud-pots, hot and cold springs) from 11 different localities in Rungwe Volcanic Province (RVP), southern Tanzania and from 3 additional localities in northern Tanzania (Oldoinyo Lengai Volcano and Lake Natron). At RVP, fluids and gases are characterized by a large range in He-isotope compositions ($^3He/^4He$) from 0.97 R_A to 7.18 R_A (where R_A = air $^3He/^4He$), a narrow range in $\delta^{13}C$ ratios from −2.8 to −6.5‰ (versus VPDB), and a large range in $CO_2/^3He$ values spanning nearly four orders of magnitude (4×10^9 to 3.2×10^{13}). Oldoinyo Lengai possesses upper-mantle-like He–CO_2 characteristics, as reported previously (Fischer et al., 2009), whereas hot springs at Lake Natron have low $^3He/^4He$ (~0.6 R_A), $CO_2/^3He$ (~5–15×10^8) and intermediate $\delta^{13}C$ (~−3.7 to −4.9 ‰). At RVP, fluid phase samples have been modified by the complicating effects of hydrothermal phase-separation, producing $CO_2/^3He$ and $\delta^{13}C$ values higher than postulated starting compositions. In contrast, gas-phase samples have not been similarly affected and thus retain more mantle-like $CO_2/^3He$ and $\delta^{13}C$ values. However, the addition of crustal volatiles, particularly radiogenic helium from ^4He-rich reservoir rocks, has modified $^3He/^4He$ values at all but the three cold CO_2 gas vent (i.e., mazuku) localities (Ikama Village, Kibila Cold Vent and Kiejo Cold Vent) which retain pristine upper-mantle He-isotope (~7 R_A) and He–CO_2 characteristics. The extent of crustal contamination is controlled by the degree of interaction within the hydrothermal system, which increases with distance from each major volcanic center. In contrast, we propose that pristine cold CO_2 mazuku gases collected at stratigraphic contacts on the flanks of RVP volcanoes may potentially tap isolated gas pockets, which formed during previous eruptive events and have remained decoupled from the local hydrothermal system. Furthermore, by identifying and utilizing unmodified gas samples, we determine mantle versus crustal provenance of the CO_2, which we use to estimate mantle-derived CO_2 fluxes at both Rungwe and Lake Natron. Finally, we investigate the origin of the apparent discrepancy in He isotopes between fluids/gases and mafic phenocrysts at RVP (from Hilton et al., 2011), and discuss the tectonic (i.e., rift zone dynamics) and petrogenic conditions that distinguish RVP from other plume-related subaerial rift zones.

1. Introduction

There is continuing debate on the source of intra-plate volcanism along the East African Rift System (EARS). Geochemical (Ebinger et al., 1989a; Furman, 1995; Marty et al., 1996; Scarsi and Craig, 1996; Furman et al., 2004; Furman, 2007; Hilton et al., 2011) and geophysical (Burke, 1996; Ebinger et al., 1997; Nyblade et al., 2000; Park and Nyblade, 2006; Adams et al., 2012) evidence suggests EARS volcanism is associated with contributions from a single mantle plume, and that the two broadly uplifted regions of the EARS (i.e., the Ethiopian and Kenyan domes; Fig. 1A) represent surface expressions of the African Superplume, which originates at the core–mantle boundary (e.g., Ebinger and Sleep, 1998; Ritsema et al., 1999). In contrast, multiple plumes could potentially be supplying magma and volatiles to various segments of the EARS (e.g., George et al., 1998). Rogers et al. (2000) presented radiogenic isotope evidence which suggests that two distinct plumes are present under these two adjacent uplifted provinces. Another possibility is that volcanism along the EARS may be associated with several heterogeneous mantle sources, including significant upper-mantle (e.g., metasomatized subcontinental lithospheric mantle and/or depleted upper mantle) contributions. In this respect, major and trace element data (Furman, 1995) and radiogenic (Sr–Nd) isotope results from the Kenyan Dome region (e.g., Rogers, 2006; Chakrabarti et al., 2009) suggest that melts are derived from metasomatic provinces within the sub-continental lithospheric mantle (SCLM): consequently,

* Corresponding author.
E-mail address: pbarry@ucsd.edu (P.H. Barry).

0009-2541/$ – see front matter © 2012 Elsevier B.V. All rights reserved.
doi:10.1016/j.chemgeo.2012.07.003

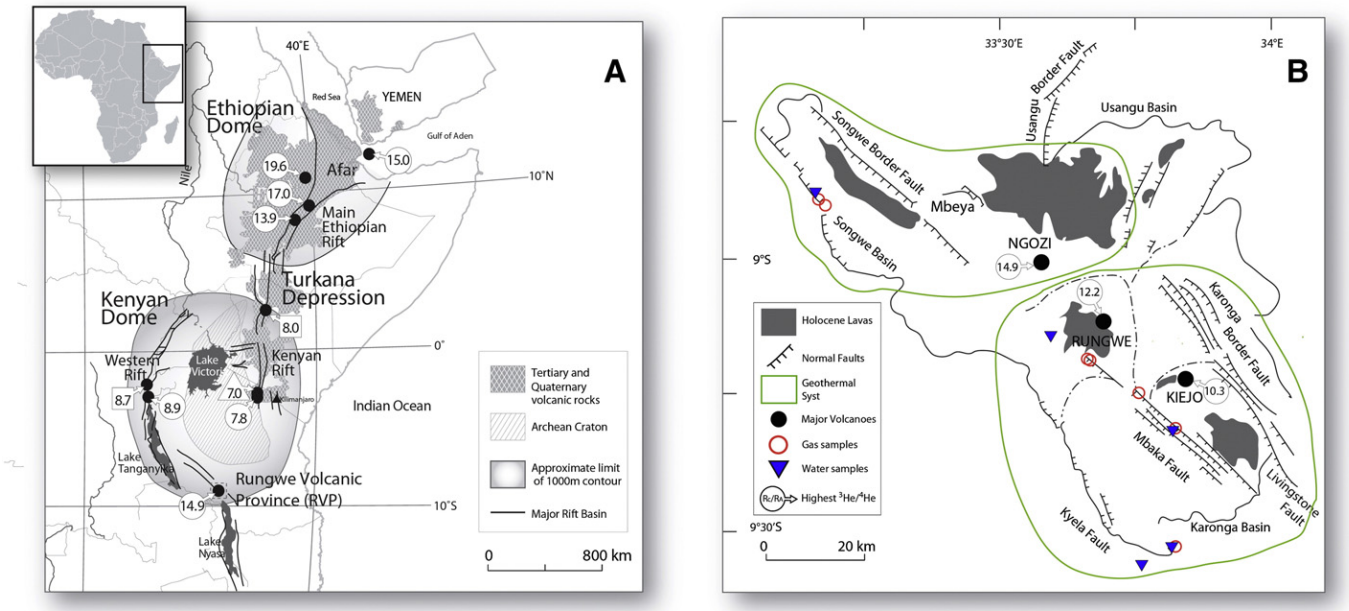

Fig. 1. A — Left: the location of the EARS (after Hilton et al., 2011). The highest reported $^3He/^4He$ ratios are plotted for various segments of the EARS, using circles (lavas), squares (hydrothermal fluids) and triangles (xenoliths). In the Western Rift of the Kenyan Dome region, $^3He/^4He$ ratios do not exceed canonical MORB values (8 ± 1 R_A) with the exception of high $^3He/^4He$ phenocryst values from RVP (Hilton et al., 2011). In addition, high He-isotopes ($^3He/^4He >$ MORB) are observed in the Ethiopia Dome, nearly 2000 km north of RVP (Scarsi and Craig, 1996) and extend throughout the Afar region to the Gulf of Aden, Red Sea and Yemen (Marty et al., 1996). B — Right: enlarged map of RVP with sample locations, fault systems, lava outcrops, major volcanoes and the main hydrothermal systems (e.g., Ngozi-Songwe in the north, Kiejo-Mbaka in the south). Open red circles denote gas samples and blue inverted triangles represent fluids samples. For reference, the highest measured $^3He/^4He$ values (Hilton et al., 2011) at RVP are shown inside circles for each of the three main volcanic centers.

volcanism in this region has been largely attributed to melting in the uppermost mantle.

Helium isotopes ($^3He/^4He$) serve as sensitive tracers of volatile provenance and are used to differentiate between various mantle and crustal sources. The $^3He/^4He$ ratio of well-mixed asthenospheric upper mantle, as sampled by mid ocean ridge basalts (MORB), is uniform at 7 to 9 R_A (where R_A = the atmospheric $^3He/^4He$ ratio of 1.4×10^{-6}). Typical SCLM values are slightly lower and range from 5.2 to 7.0 R_A (Gautheron and Moreira, 2002). Similarly, continental intraplate alkaline volcanics (CIAV) range from 5.3 to 6.7 R_A (Day et al., 2005). In contrast, many mantle plume regions (e.g., Iceland, Hawaii, Samoa — see review by Graham, 2002) show a marked relative enrichment in ^3He, with values extending as high as ~50 R_A (e.g., Stuart et al., 2003). Such high values are consistent with a mantle reservoir with a high time-integrated $^3He/(U+Th)$ ratio, which has remained largely undegassed since Earth's accretion. In stark contrast, continental crust is characterized by low $^3He/^4He$ ratios of ~0.05 R_A (Morrison and Pine, 1955) due to production of radiogenic He. Large variations in $^3He/^4He$ ratios between mantle and continental reservoirs (>three orders of magnitude) form the basis for the utility of helium isotopes as a tracer of mantle-derived volatiles.

Helium isotopes have been extensively studied throughout the EARS: the Ethiopian Dome is marked by a large range in He-isotopes with the highest $^3He/^4He$ values in the EARS (up to 19.6 R_A) suggesting significant plume-like contributions (Marty et al., 1996; Scarsi and Craig, 1996), whereas $^3He/^4He$ ratios throughout the Kenyan Dome were, until recently, consistently MORB-like (8 ± 1 R_A) or lower, indicating an asthenospheric upper mantle or SCLM source, with crustal assimilation resulting in $^3He/^4He$ values well below 8 R_A (Darling et al., 1995; Pik et al., 2006; Hopp et al., 2007; Fischer et al., 2009; Tedesco et al., 2010). However, Hilton et al. (2011) reported high He-isotope ratios (up to ~15 R_A) at RVP at the southernmost extent of the EARS. These new He-isotope data imply that mantle source(s) of volatiles at RVP, and by inference the Kenyan Dome region as a whole, are no longer constrained to the upper mantle alone.

In this contribution, we target fluids and gases at RVP – and from two locations in northern Tanzania – to characterize the regional He isotope systematics as well as C-isotope (CO_2) and relative abundance features. In part, our motivation is to add to the He isotope database already established for the region (Pik et al., 2006) whereby the hydrothermal fluids and gases appeared to only sample $^3He/^4He$ ratios equal to or less than MORB — in contrast to higher values recently measured in mafic phenocrysts at RVP (Hilton et al., 2011). In addition, we report new C-isotope (CO_2) values in order to ascertain the characteristics and provenance of this major volatile phase. Furthermore, by combining He and CO_2 measurements of the same gas/fluid samples, we are able to identify potentially complicating factors (e.g., phase separation, fluid mixing) related to utilizing hydrothermal systems versus cold CO_2 (mazuku-like) vents which are also found at RVP. As these cold CO_2 vents have He–CO_2 characteristics distinct from hydrothermal samples, we suggest that they may represent storage and release sites located within the volcanic stratigraphy, which are, for the most part, independent of any regional or local hydrothermal system. Finally, using the combined He–CO_2 approach, we are able to offer an explanation for the apparent He-isotope discrepancy observed at RVP when hydrothermal fluids and mafic phenocrysts are used independently to infer He isotope characteristics of the mantle source region.

2. Geological background

The EARS is the classic example of modern continental rifting, with extension accommodated by faulting, crustal thinning, and volcanism (e.g., Dawson, 2008). The rift stretches from the Afar Depression in northern Ethiopia/Eritrea to RVP in southern Tanzania (Fig. 1A). It crosses the Ethiopian Dome before splitting into two main branches (Western and Kenyan rifts), encircling the Tanzanian craton located on the Kenyan Dome and forming a triple junction at RVP (Delvaux and Hanon, 1993; Mnjokava, 2007). Rift initiation began in southern Ethiopia at approximately 45 Ma (George et al, 1998) and was followed by volcanism in northern Ethiopia and Yemen at approximately 30 Ma

(Schilling et al, 1992; Pik et al, 1999). Present-day magmatic activity occurs intermittently along the ~2000 km rift, which spans pre-rift, syn-rift, and post-rift periods. Volcanic activity at RVP dates from 8.6 Ma to the present (Ebinger et al., 1989b, 1993; Ebinger and Furman, 2003).

The geology of Tanzania is dominated by the Precambrian Tanzania Craton (>2 Ga) bounded by Proterozoic metamorphic and intrusive rocks marking the intersection of three distinct Proterozoic mobile belts: the Ubendian, Irumide, and Mozambique belts (Harkin, 1960). Inland Tanzanian basins are filled with Cenozoic sediments and volcanic rocks associated with rifting of the EARS. RVP is located directly south of the Tanzanian Craton (Fig. 1B) and covers an area of ~1500 km^2. It is located at the intersection of the Karonga, Songwe, and Usangu basins (Fig. 1) (Harkin, 1960; Delvaux and Hanon, 1993). The Karonga basin is the northernmost sub-basin of the Malawi rift (Ebinger et al., 1987), and is comprised of Precambrian basement rocks overlain by basalt, trachyte, and phonolite from the northern volcanic highlands, and by both Permian–Triassic and younger (Neogene) sediments of the Kyela lowlands. RVP consists of asymmetric half grabens which accommodate the overall WSW–ENE extension (Ebinger et al., 1989b; Iranga, 1992; Delalande et al., 2011) and NW–SE trending normal faults which are manifested in three main rift-bounding fault segments: Kyela, Mbaka and Livingstone faults (Hochstein et al., 2000) (Fig. 1B).

Late Miocene to Quaternary volcanism and associated hydrothermal activity characterize recent magmatism at RVP (Ebinger et al., 1989b). RVP is comprised of three main volcanic centers: Ngozi, which last erupted <1 ka before present (trachytic tuff); Rungwe volcano, which last erupted <1.2 ka before present (trachytic tephra); and Kiejo, which last erupted a tephrite lava flow <0.2 ka before present (tephrite lava flow) (Harkin, 1955; Ebinger et al., 1989b; Fontijn et al., 2010a, 2010b, 2011). In addition, the region hosts abundant smaller monogenic volcanoes and cinder cones located along the Mbaka fault, which were constructed during the last 0.5 Ma (Ebinger et al., 1989b; Williams et al., 1993; Fontijn et al., 2010b).

Hydrothermal activity occurs throughout RVP and is marked by abundant bubbling springs, located along streambeds and riverbanks believed to be connected to groundwater aquifers by an extensive fault network (Delalande et al., 2011). Fluids are characterized as Na–HCO_3 waters, with variable Ca–Mg and Cl contributions (Harkin, 1960; Hochstein et al., 2000; Branchu et al., 2005; Kraml et al., 2010; Delalande et al., 2011), and all show evidence for the degassing of CO_2 (Ebinger et al., 1993). Based on sample location and field observations (i.e., temperature, salinity and pH), RVP hydrothermal activity is divided into two main groups (Delalande et al., 2011):

(1) A group of cold gas-rich bubbling springs which is located at high elevations (1500–1700 m). These freshwater, Na (Ca–Mg)–HCO_3 type, springs display low temperatures (15 to 23 °C), are slightly acidic (pH between 5.2 and 6.7) and show intense gas bubbling. In addition, vigorously degassing cold CO_2 vents have also been reported on the flanks of Ngozi, Rungwe and Kiejo volcanoes (Delalande et al., 2011).
(2) A group of hot gaseous springs is located at lower elevations (500–800 m) in the Kyela plain and lies on or close to major active NW–SE faults. Spring temperatures range from 32 to 63 °C suggesting connection to low enthalpy thermal activity (Arnórsson, 2000). Waters are saline, Na–HCO_3(Cl) type, and display neutral to slightly basic pH (7.0–7.9) (Delalande et al., 2011). Significantly, hot springs show weaker gas activity (generally fewer/smaller bubbles, higher water flows) than the higher elevation cold springs and gas vents.

This second group of hot springs has been further sub-divided into two distinct hydrothermal systems on the basis of fluid chemistry and geographic extent (Kraml et al., 2010): (a) Ngozi-Songwe hydrothermal system, located in the NW, and (b) Kiejo-Mbaka hydrothermal system, in the south (Fig. 1B). Each hydrothermal is described in turn:

The Ngozi-Songwe hydrothermal area is located to the NW of Ngozi volcanic center and 30 km west of Mbeya (Fig. 1A). The Songwe hot spring area is located ~43 km NW of the Ngozi volcanic center and is the most thermally-active and best-studied hydrothermal area in Tanzania: its thermal output is approximately 10 MW (Hochstein et al., 2000; Kraml et al., 2010). Volcanological investigations suggest that a trachytic magma chamber of Ngozi volcano provides an ideal heat source for the region (Kraml et al., 2010). In addition, Songwe is marked by hot Na-bicarbonate springs, CO_2 vents and extensive travertine deposits (~150 million tons) (Kraml et al., 2010). Together, the chemical composition of the thermal waters, the CO_2 discharge of the springs, and the presence of travertine, indicate that Songwe hot springs mark the terminus of a concealed outflow of hot water, channeled by a confined aquifer (Hochstein et al., 2000). Tectonic investigations show that fluid flow is fault controlled. Furthermore, hydrological investigations have determined that recharge for the Songwe hydrothermal fluids occurs at elevations between 1800 and 2200 m, likely near the Ngozi volcanic summit (James, 1967; Delvaux et al., 2010; Kraml et al., 2010).

The Kiejo-Mbaka hydrothermal system encompasses both the Kiejo and Rungwe volcanic centers. Kiejo is located ~36 km NW of Lake Malawi at an elevation of approximately 2200 m (Fig. 1B). The Rungwe volcanic center is located approximately 20 km to the northwest of Kiejo and is comprised of mostly alkali-basaltic and trachytic/phonolitic rocks of Miocene to Quaternary age (Hochstein et al., 2000). The most prominent structure within the Kiejo-Mbaka hydrothermal system is the Mbaka fault, which crosscuts the volcanoes and serves as a permeable conduit for gas and hydrothermal fluid activity (Hochstein et al., 2000). Springs and gases principally emanate from sites where disconnected or recently reactivated conjugate faults cross the Mbaka fault system (Kraml et al., 2010). Fluid chemistry (i.e., Na and HCO_3 contents and Na/K ratios) indicates a homogenous fluid at depth (Mnjokava, 2007), with both the relatively high heat-flow and chemistry of hot springs consistent with the presence of a significant magmatic intrusion driving the system (Branchu et al., 2005).

3. Samples and analytical techniques

We sampled a total of 7 localities from the two high temperature hydrothermal systems (i.e., Ngozi-Songwe and Kiejo-Mbaka) and 4 sites of cold CO_2 vents/springs. In total, 20 samples (7 fluid-phase and 13 gas-phase) were collected, with duplicate (or triplicate) samples taken at 8 of the 11 localities. In addition, we sampled 3 localities (4 fluid-phase and 2 gas-phase samples) in the Oldoinyo Lengai/Lake Natron region of northern Tanzania (Table 1). All samples (n = 26) were collected in evacuated 1720-glass bottles using standard sampling techniques (e.g., inverted funnel) in order to minimize possible air contamination (see Hilton et al., 2002 for details).

Within the Ngozi-Songwe hydrothermal system, 4 samples were collected from 3 distinct bubbling hot (54–71 °C) spring sites — both in and immediately adjacent to a travertine quarry located ~40 km NW of the Ngozi volcanic center (Songwe Overlook, Mesa and Quarry). A total of 4 hot (36–70 °C) spring sites were targeted in the Kiejo-Mbaka hydrothermal system: Kilambo Springs, located ~16 km S of the Kiejo volcanic center, and three springs in the Mampulo and Kasimulo springs region located ~50 km SSE of the Rungwe volcanic center.

Additionally, we collected gases from three vigorously degassing dry CO_2 cold (12–23 °C) vents on the flanks of Kiejo and Rungwe volcanoes, at the contact between basaltic flows and phonolitic tuff units, and one cold (20 °C) spring (Kafwira Njuni) from the flank (~9 km W) of Rungwe volcano (Harkin, 1960). The Kiejo Cold Vent sample was collected <5 km from the summit of Kiejo, close to the factory where CO_2 gas is commercially extracted from three shallow boreholes (Hochstein et al., 2000). Two cold CO_2 vents near Ikama Village (Kibila and Ikama Village

Table 1
Helium and carbon isotope and relative abundance characteristics of hydrothermal fluids and gases from RVP and northern Tanzania.

Sample location	Phase[a]	Latitude (°S)	Longitude (°E)	Elevation (m)	Distance to volcano[b] (km)	Temp (°C)	R/R_A[c]	X[d]	R_C/R_A[e]	$CO_2/^3He$ ($\times 10^9$)[f]	$\delta^{13}C$ (‰)[g]	$[CO_2]$ (mmol/kg)	[He] ($\mu cm^3/gH_2O$)
Rungwe Volcanic Province (RVP)													
Ngozi-Songwe hydrothermal system													
Songwe Overlook	F	08° 52′ 16.3″	33° 10′ 52.7″	1137	43 (N)	71	1.19	2.63	1.28 ± 0.05	2300	−4.37	35.0	0.222
Songwe Mesa	G	08° 52′ 23.9″	33° 10′ 52.6″	1,137	43 (N)	64	3.61	18.7	3.73 ± 0.12	35.5	−5.36	–	–
(Dup)							3.75	527	3.75 ± 0.09	22.7	−6.10	–	–
Songwe Quarry	G	08° 53′ 21.6″	33° 12′ 37.9″	1177	40 (N)	54	1.21	1.88	1.38 ± 0.07	2350	−5.92	–	–
Kiejo-Mbaka hydrothermal system													
Kilambo Springs	F	09° 21′ 43.7″	33° 49′ 01.3″	637	16 (K)	57	0.97	3.19	0.97 ± 0.09	32,200	−3.77	48.7	0.032
Kilambo Springs	G	09° 21′ 44.0″	33° 49′ 01.5″	637	16 (K)	36	3.65	85.6	3.67 ± 0.11	57.9	−5.43	–	–
Mampulo Spring #1	F	09° 33′ 01.9″	33° 47′ 49.6″	515	50 (R)	60	2.00	19.4	2.05 ± 0.10	2420	−4.81	56.4	0.341
(Dup)							2.05	28.3	2.08 ± 0.09	1680	−5.34	53.8	0.703
Mampulo Spring #2	G	09° 33′ 01.9″	33° 47′ 43.8″	523	50 (R)	55	2.20	9480	2.20 ± 0.07	3.05	−6.45	–	–
(Dup)							2.13	10,400	2.13 ± 0.07	2.94	−6.01	–	–
(Dup)							2.10	4220	2.01 ± 0.06	3.21	−6.41	–	–
Kasimulo Spring	F	09° 34′ 52.7″	33° 45′ 42.2″	520	53 (R)	52	1.04	2.48	1.06 ± 0.05	6660	−2.79	47.5	0.100
(Dup)							1.02	1.96	1.03 ± 0.06	12,200	−3.14	48.8	0.058
Cold CO_2 mazuku vents and bubbling springs													
Kafwira Njuni	F	09° 08′ 12.5″	33° 35′ 17.5″	1552	9 (R)	20	4.49	3.63	5.49 ± 0.23	320	−4.12	19.6	0.178
Ikama Village	G	09° 12′ 41.6″	33° 39′ 14.2″	1505	10 (R)	23	6.31	15.9	6.60 ± 0.12	4.53	−4.56	–	–
(Dup)							7.16	269	7.18 ± 0.13	4.46	−5.17	–	–
Kibila Cold Vent	G	09° 12′ 54.3″	33° 39′ 28.8″	1490	11 (R)	12	7.09	4950	7.09 ± 0.20	4.00	−4.24	–	–
(Dup)							7.08	298	7.09 ± 0.20	4.53	−3.89	–	–
Kiejo Cold Vent	G	09° 15′ 03.8″	33° 45′ 43.2″	1504	4 (K)	15	6.12	870	6.12 ± 0.17	3.85	−4.43	–	–
(Dup)							6.61	2570	6.61 ± 0.11	5.34	−4.96	–	–
Northern Tanzania (Lengai/Lake Natron)													
Lake Natron #2	F	02° 23′ 23.2″	35° 53′ 50.9″	620	–	50	0.64	5890	0.64 ± 0.02	1.53	−4.02	15.1	300
(Dup)							0.67	12, 800	0.67 ± 0.02	0.48	−4.42	16.2	724
Lake Natron #1	F	02° 22′ 14.2″	35° 54′ 17.7″	608	–	51	0.63	7170	0.63 ± 0.02	1.12	−4.92	15.1	209
(Dup)							0.61	5510	0.61 ± 0.02	1.21	−3.70	17.4	331
Lengai North Crater	G	02° 45′ 22.6″	35° 54′ 41.2″	2827	–	70	6.76	6530	6.77 ± 0.16	2.60	−2.43	–	–
(Dup)							70	6.87	1210	6.88 ± 0.20	2.91	−2.77	–	–

All reported errors are at the 1sigma level.
[a] Fluid (F), Gas (G).
[b] Volcanic center: (N) = Ngozi, (K) = Kiejo, (R) = Rungwe.
[c] R/R_A is measured $^3He/^4He$ ratio divided by the $^3He/^4He$ in air $= 1.4 \times 10^{-6}$.
[d] X-value (gas) $= (^4He/^{20}Ne)_{measured}/(^4He/^{20}Ne)_{air}$. X-value (fluid) $= (^4He/^{20}Ne)_{measured}/[(^4He/^{20}Ne)_{air} \times (\beta_{Ne}/\beta_{He})]$, where β = Bunsen solubility coefficient. For pure water at 15 °C $(\beta_{Ne}/\beta_{He}) = 1.22$ (Weiss, 1971). See Hilton (1996) for further details of the correction protocol.
[e] R_C/R_A is the air corrected He isotope ratio $= [(R/R_A \times X) - 1]/(X - 1)$.
[f] Accuracy is estimated to be better than 5%.
[g] Accuracy is ±0.5‰.

samples), located <9 km from the summit of Rungwe volcanic center, were also sampled. All three cold CO_2 vent features show remarkable similarities to "mazuku", previously described along parts of the western branch of the EARS, in the Goma region of the Democratic Republic of Congo (Smets et al., 2010). Mazuku means "evil-wind" in Swahili and is used to describe lowland (depressions) where CO_2 is released to the atmosphere. Being heavier than air, CO_2 can accumulate in depressions at high and often lethal levels (Tuttle et al., 1990; Smets et al., 2010). Notably, mazuku from the Lake Kivu region (western branch of EARS) display mantle helium isotope values and have thus been unambiguously linked to an upper-mantle source (Tedesco et al., 2010). These cold CO_2 mazuku-like vents are grouped with Kafwira Njuni cold spring in Table 1 as they share low temperatures (<23 °C); however, it is not obvious that they are related to localized hydrothermal systems (see Section 5.3).

Finally, three northern Tanzania sites were sampled (Table 1). The hyper-saline Lake Natron is located towards the southern end of the Kenyan Rift, about 45 km north of Oldoinyo Lengai volcano, and discharges numerous warm springs (32–52 °C) along the shoreline (Hochstein et al., 2000). Two warm springs located along a shoreline scree slope were sampled. Additionally, we collected moderate temperature gases (~70 °C) from a fumarole on the outer summit crater wall of Oldoinyo Lengai volcano at an elevation ~2800 m. Details on sampling locations – latitude, longitude, elevation and distance to nearest volcanic edifice – are included in Table 1.

Helium, Ne and CO_2 were extracted from all samples at the Fluids and Volatiles Laboratory, Scripps Institution of Oceanography (SIO), using a dedicated UHV purification line (see Kulongoski and Hilton, 2002 for description). Following sample inlet into the vacuum system, waters were acidified with phosphorus pentoxide to ensure complete release of CO_2; consequently, CO_2 amounts represent the total dissolved inorganic carbon (TDIC) content. Water vapor was isolated on a water-trap held at −78 °C (cooled using a slurry of acetone and dry-ice). Subsequently, CO_2 was frozen onto a liquid nitrogen cooled U-tube. The remaining light noble gases (He and Ne) were then isolated using a hot (700 °C) Ti-getter and charcoal finger held at liquid nitrogen temperature, which acted to remove active gases (N_2, CO, and CH_4) and heavy noble gases (Ar, Kr and Xe), respectively. A calibrated fraction of the He and Ne gas was captured in an AR-glass breakseal for transfer to a MAP-215 noble gas mass spectrometer. Finally, the CO_2 fraction was transferred to a Pyrex breakseal for transfer to a dedicated CO_2 cleanup line.

The He and Ne gas fraction was released from the breakseal and prepared for inlet into the MAP-215 mass spectrometer using a combination of charcoal traps held at liquid nitrogen temperature and active-gas getters. Following this initial clean-up, a helium-cooled cryogenic trap was used to separate He from Ne, which were inlet sequentially into the mass spectrometer. The measured $^3He/^4He$ ratio of the sample was normalized to standard aliquots of air run before and after each sample analysis.

The carbon dioxide (CO_2) sample fraction was transferred to a secondary clean-up and quantification line, constructed from Pyrex glass, where CO_2 and any sulfur-bearing species (if present) were separated using a variable temperature trap. Following clean-up, the total amount of CO_2 was measured using a capacitance manometer in a calibrated volume. The manometrically-derived CO_2 abundance was then combined with the mass spectrometer-derived $^3He/^4He$ value and helium abundance to calculate the $CO_2/^3He$ ratio. Following manometric measurement, CO_2 was again frozen into a Pyrex tube for transfer to a Thermo Finnigan Delta XP_{plus} isotope ratio mass spectrometer for carbon isotopic ($\delta^{13}C$) analysis. δ^{13} (CO_2) values are reported relative to the international reference standard Vienna Pee Dee Belemnite (VPDB) and have a precision of less than 0.1‰. We estimate the accuracy of our $\delta^{13}C$ determinations ($\pm$0.5‰) by repeat analyses of a working laboratory standard, itself calibrated relative to VPDB.

4. Results

4.1. Helium isotopes ($^3He/^4He$ ratios)

Helium isotope results ($^3He/^4He$ ratios = R) are reported relative to air (R_A) (where R_A = atmospheric $^3He/^4He = 1.4 \times 10^{-6}$) and corrected for the presence of atmospheric He (to R_C/R_A). By monitoring sample $^4He/^{20}Ne$ ratios, and assuming all sample ^{20}Ne is derived from air or air saturated water, the atmospheric He contribution can be calculated and subsequently subtracted from the measured value. The air–He correction is based on known $^4He/^{20}Ne$ values of air or air saturated water (adjusted for He and Ne solubility variations in water – assuming a recharge temperature of 15 °C – for fluid samples only) (Ozima and Podosek, 1983; Hilton, 1996). Relative $^4He/^{20}Ne$ enrichments versus air are expressed as X-values (where $X = (He/Ne)_S/(He/Ne)_A$). X-values vary by over 4 orders of magnitude in RVP and northern Tanzania samples (Fig. 2) and are markedly higher in gas-phase versus fluid phase samples. We note the following two general features of the helium data: (a) duplicate samples (i.e., same phase and locality) are in excellent agreement and deviate by less than 0.2 R_A for all samples except Ikama Village, where duplicates vary by 0.58 R_A, and (b) fluid-phase samples display lower $^3He/^4He$ values than gas-phase samples from the same site.

At RVP, helium isotope ratios cover a wide range (0.97 R_A to 7.18 R_A), and are in good agreement with earlier reports of He isotopes (0.22 R_A to 7.76 R_A) from the region (Pik et al., 2006) (Fig. 3). For example, we report a $^3He/^4He$ value of 7.2 R_A from Ikama Village, in good agreement with that reported by Pik et al. (2006). In detail, we point out the following salient features of the air-corrected He isotope results:

1. Cold CO_2 mazuku vents range from 6.1 to 7.2 R_A with the cold fluid-phase sample from Kafwira Njuni having a $^3He/^4He$ value of 5.5 R_A. These ratios are consistently the highest values in this study.
2. Localities in the Kiejo-Mbaka hydrothermal system range in $^3He/^4He$ from 0.97 (fluid phase at Kilambo Springs) to 3.67 R_A (corresponding gas phase at the same locality). Mampulo Spring samples (2 locations) range from 2.0 to 2.2 R_A whereas Kasimulo Spring fluids overlap with the atmospheric value (1 R_A) within analytical uncertainty.
3. In the Ngozi-Songwe hydrothermal system, $^3He/^4He$ ratios at Songwe range from 1.3 (fluid phase) to 3.75 R_A and display evidence for both mantle and radiogenic contributions to the total He inventory.

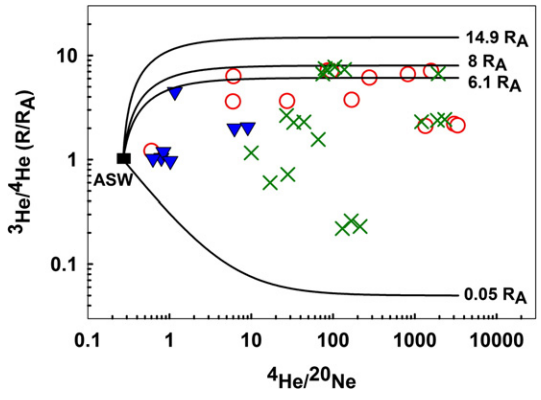

Fig. 2. He-isotopes versus $^4He/^{20}Ne$ data for hydrothermal fluids (blue inverted triangles) and gases (red open circles) from RVP. Data are shown with previously reported hydrothermal fluid data (green X's) from Pik et al. (2006). Calculated binary mixing lines between air saturated water (ASW), crustal and mantle endmember compositions are shown. Endmembers are: ASW $^3He/^4He = 1$ R_A, $^4He/^{20}Ne = 0.250–0.285$; (Ozima and Podosek, 1983), High $^3He/^4He = 14.9$ R_A, (Hilton et al., 2011), MORB $^3He/^4He = 8$ R_A, (Graham, 2002), SCLM $^3He/^4He = 6.1$ R_A, (Gautheron and Moreira, 2002) Crustal $^3He/^4He = 0.05$ R_A (Morrison and Pine, 1955): in the latter 4 cases a $^4He/^{20}Ne$ ratio ~3500 is assumed.

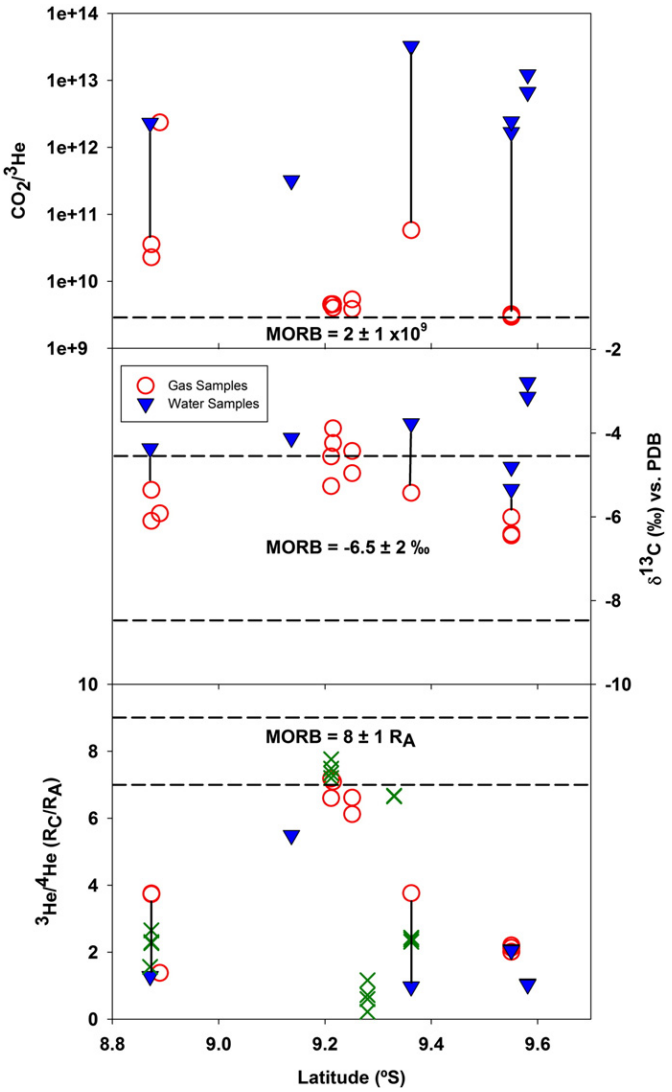

Fig. 3. Helium and carbon isotope ($^3He/^4He$ — corrected for air and given in R_C/R_A notation; $\delta^{13}C$) and relative abundances ($CO_2/^3He$) plotted versus latitude for all 11 RVP localities sampled. Open red circles represent gas-phase samples and solid blue triangles represent fluid-phase samples. In addition, hydrothermal fluid He-isotopes (from Pik et al., 2006) are shown (green X's). Vertical tie-lines connect gas and fluid phase samples from the same locality. Horizontal dashed lines delineate typical MORB ranges for carbon and helium isotopes.

We also note that there is a distinct peak in $^3He/^4He$ values at 9.2°S (Fig. 3), which is associated with the location of the cold CO_2 mazuku vents (Ikama Village, Kibila and Kiejo Cold Vent samples) near the termination of the Mbaka fault system in the central region of the Kiejo-Mbaka hydrothermal system. In summary, the most prominent characteristic of RVP helium isotope results is that all samples are characterized by a mantle-derived contribution (Section 5.4). The highest values fall at the lower end of the range normally associated with mid-ocean ridge basalt (MORB) helium (8 ± 1 R_A) whereas the lowest ratios, although having a large proportion of radiogenic helium, are still well above the radiogenic He production ratio (0.05 R_A) (Morrison and Pine, 1955).

In addition, we report $^3He/^4He$ values for northern Tanzania samples (Lake Natron and Oldoinyo Lengai). Lake Natron springs cluster tightly between 0.61 to 0.67 R_A, showing a strong radiogenic He signal. In contrast, the Oldoinyo Lengai fumarole has a $^3He/^4He$ ratio of 6.88 R_A, in good agreement with fumaroles sampled in 2005 (~6.86 R_A; Fischer et al., 2009) prior to the 2007 eruptive events.

4.2. Carbon isotopes ($\delta^{13}C$ (CO_2))

C-isotopes ($\delta^{13}C$) range from −2.8 to −6.5‰ (versus VPDB) at RVP and from −2.4 to −4.9‰ (versus VPDB) in northern Tanzania, with all values falling within or slightly higher than the range normally associated with MORB (-6.5 ± 2‰) (Sano and Marty, 1995). Agreement between duplicate samples is at the level of ~1.2‰ or less.

The Ngozi-Songwe hydrothermal system C-isotope compositions range from −4.4 to −6.1‰, with overlap (within uncertainty) between the Mesa and Quarry localities. The range of $\delta^{13}C$ values is much greater for the Kiejo-Mbaka hydrothermal system with the highest $\delta^{13}C$ value (−2.8‰) observed at Kasimulo springs, in a fluid sample with a $^3He/^4He$ value overlapping with air, and the lowest $\delta^{13}C$ value (−6.5‰) measured in a gas-phase sample from Mampulo Springs #2 with a higher $^3He/^4He$ ratio (2.2 R_A) and negligible air addition (X = 9475).

The cold gas vents range from −3.9 to −5.2‰ with the single fluid phase sample (Kafwira Njuni) having an intermediate value (−4.1‰). Three localities at RVP have both fluid and gas-phase samples with $\delta^{13}C$ data (see samples connected by tie-lines in Fig. 3). In each case, carbon isotope values were significantly higher in the fluid phase. Unlike He-isotopes, there is no clear latitudinal control on the range of ($\delta^{13}C$) values (Fig. 2).

At Lake Natron, $\delta^{13}C$ values fall between −4.9 and −3.7‰ with duplicate values in good agreement and overlapping within uncertainty at location #2. The Oldoinyo Lengai fumarole $\delta^{13}C$ values are higher than at Natron (−2.3 to −2.8‰) and again overlap within analytical uncertainty (0.5‰). They fall within the range of values reported for summit fumaroles collected in 2005 (Fischer et al., 2009).

4.3. $CO_2/^3He$ ratios

The elemental $CO_2/^3He$ ratio varies over 4 orders of magnitude in RVP samples, from ~3×10^9 (MORB-like) to higher values (~3×10^{13}) normally associated with crustal lithologies (O'Nions and Oxburgh, 1988). By comparison, northern Tanzania samples span a more limited range, extending from 5×10^8 to 3×10^9, at the MORB range or lower.

The Ngozi-Songwe hydrothermal system $CO_2/^3He$ values range from 22.7 to 2350 ($\times 10^9$), with good agreement of low values, 23 and 36 ($\times 10^9$), at the Mesa locality and between the Overlook and Quarry sites (2300 and 2350) ($\times 10^9$). Kiejo-Mbaka hydrothermal system $CO_2/^3He$ values span a greater range, with values falling between 2.94 and 32,200 ($\times 10^9$). Several gas samples at Mampulo Springs have $CO_2/^3He$ values that fall within the MORB-range ($2 \pm 1 \times 10^9$; Marty and Jambon, 1987) whereas all other samples (i.e., both fluid and gas phases) are significantly higher.

Cold CO_2 mazuku vent $CO_2/^3He$ values are consistently low, between 3.85 and 5.34 ($\times 10^9$) whereas the cold fluid-phase sample (Kafwira Njuni) has a $CO_2/^3He$ value of 320 ($\times 10^9$). In general, fluid samples at RVP have significantly higher $CO_2/^3He$ values, ranging from 3.2×10^{11} to 3.2×10^{13}, compared with the range in corresponding gas samples (3×10^9 to 2×10^{12}). The three localities where both fluid and a gas samples were collected display much higher $CO_2/^3He$ ratios in the fluid-phase samples (see samples with tie-lines in Fig. 3), indicating that the fluids may reflect modified $CO_2/^3He$ characteristics (see Section 5.2 for discussion).

At Lake Natron, the $CO_2/^3He$ values are consistently low, with values between 4.8×10^8 and 1.5×10^9. Whereas there is poor agreement for site #2 samples, this is not the case for site #1 where values are 1.1 and 1.2 ($\times 10^9$). Such low values are unusual given the low $^3He/^4He$ ratios at these localities indicative of a significant crustal (radiogenic) He input: this observation may reflect loss of CO_2 (Section 5.2.2). The $CO_2/^3He$ values at Oldoinyo Lengai fall within the MORB range and are slightly lower than values published previously for summit fumaroles (Fischer et al., 2009).

5. Discussion

In the following discussion, we investigate processes that could affect regional hydrothermal $^3He/^4He$ values (and associated He–CO_2 characteristics) and thus lead to the discrepancy in helium isotopes between fluids and phenocrysts. Our approach is to identify samples that exhibit $^3He/^4He$, $CO_2/^3He$ and $\delta^{13}C$ values representative of the mantle source region versus those whose features have been modified by other processes (i.e., magmatic and/or hydrothermal-related). In this way, volatile signatures can be utilized to understand the nature of mantle sources. A corollary of this approach allows us to focus on the He–CO_2 systematics of the three cold CO_2 mazuku-like features in the region and assess their role in transferring mantle-derived volatiles to the surface. Finally, we address the factors behind the apparent He-isotope discrepancy observed between mafic crystals of RVP lavas and tephra (Hilton et al., 2011) and geothermal gases/fluids (this work) which is conspicuously absent at other plume-related localities such as Iceland (Hilton et al., 1990).

5.1. Observed CO_2–^3He–^4He characteristics

To evaluate sample integrity (gases versus fluids), particularly regarding possible elemental fractionation effects between He and CO_2, we plot all RVP samples (n = 20) and the northern Tanzanian samples (n = 6) on a CO_2–^3He–^4He ternary diagram (Fig. 4; after Giggenbach et al., 1993). For reference, we include mixing lines showing binary mixing between mantle $^3He/^4He$ endmembers (e.g., SCLM = 6.1 ± 0.9 R_A (Gautheron and Moreira, 2002); MORB = 8 ± 1 R_A (Graham, 2002); high $^3He/^4He$ (RVP) = 15 ± 1 R_A (Hilton et al., 2011), crustal values (~0.05 R_A) (Shaw et al., 2003) and/or pure radiogenic ^4He. In the case of $CO_2/^3He$ endmembers, we adopt values of 2 ± 1 ($\times 10^9$) for MORB-mantle (Marty and Jambon, 1987), 4 ± 2 ($\times 10^9$) for SCLM (Hahm et al., 2008; Fischer et al., 2009), assuming that Oldoinyo Lengai volcano in northern Tanzania with $^3He/^4He$ ratios <7 R_A represents this component, and 10^{13} for the crustal endmember (O'Nions and Oxburgh, 1988).

In Fig. 4, we note the following features with respect to the gas phase samples from RVP:

(1) All six cold gas (mazuku) vents (e.g., duplicate samples from Kibila Cold Vent, Ikama Village and the Kiejo Cold Vent) plot within the range of MORB/SCLM $^3He/^4He$ values (8 ± 1 R_A and 6.9 ± 0.9, respectively; Graham, 2002; Gautheron and Moreira, 2002) and SCLM-like $CO_2/^3He$ ($4 \pm 2 \times 10^9$) values (Hahm et al., 2008; Fischer et al., 2009).

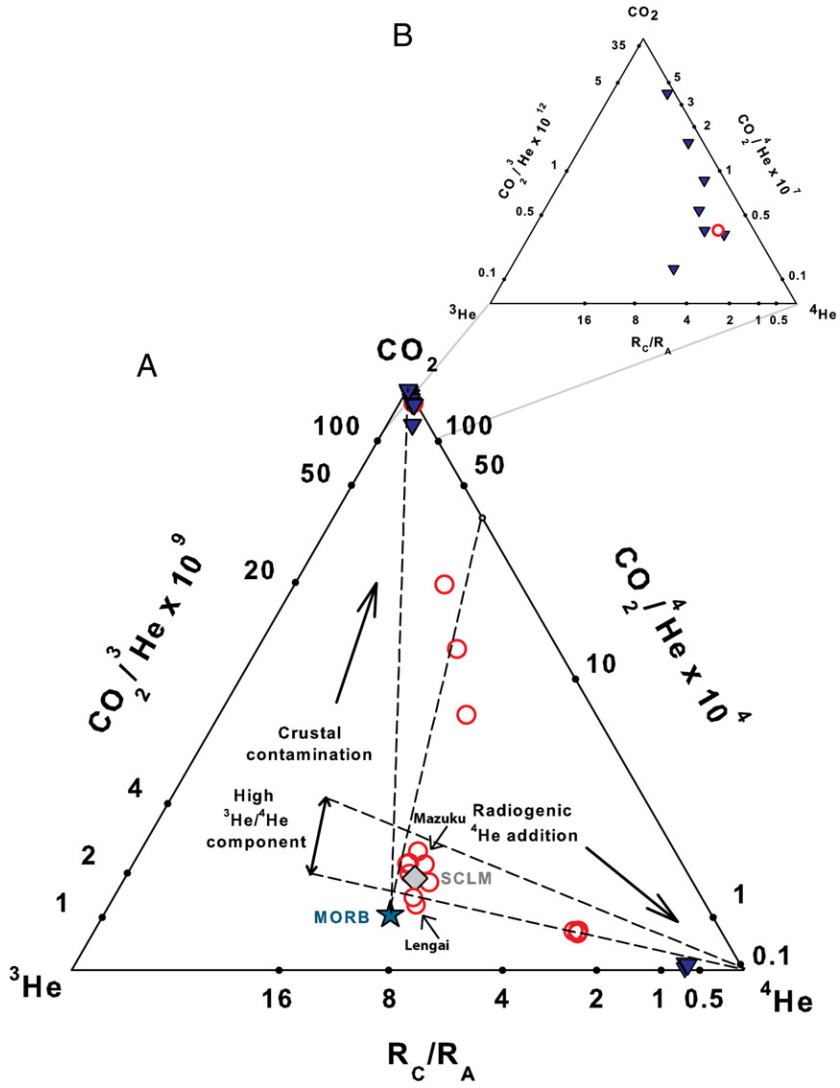

Fig. 4. A — Ternary plot of CO_2, ^3He, and ^4He for gas (open red circles) and fluid samples (blue triangles) from RVP and northern Tanzania, illustrating the effects of crustal and radiogenic contamination of mantle-like volatiles. For reference, we plot "mantle average" (MORB = 8 ± 1 R_A) with a turquoise star (Marty and Jambon, 1987), sub-continental lithospheric mantle (SCLM = 6.1 ± 0.9 R_A) with a grey diamond (Gautheron and Moreira, 2002) and "high $^3He/^4He$ component" ($CO_2/^3He$ = 3–6 × 10^9 after Poreda et al., 1992; Marty and Tolstikhin, 1998; $^3He/^4He$ = 14.9 R_A after Hilton et al., 2011). All gas samples fall on or are close to a binary mixing trajectory between upper mantle-like (MORB; SCLM) helium and variable amounts of crustal contamination (calculated from $CO_2/^3He$ = 5–50 × 10^{12}; $^3He/^4He$ = 0.05 R_A) (Shaw et al., 2003) and/or air. Fluid samples of RVP display much higher $CO_2/^3He$ (3.2 × 10^{11} to 3.2 × 10^{13}) and helium isotope values compared with northern Tanzania fluid samples (i.e. Lake Natron) which display both low $CO_2/^3He$ (< 2 × 10^9) and helium isotope values. As a result, RVP fluid samples plot close to the CO_2 apex whereas Lake Natron samples plot close to the ^4He apex. B — Ternary plot of CO_2, ^3He, and ^4He, with different scale axes focused on the CO_2 apex in order to show fluid-phase samples from RVP. Fluid samples of RVP display much higher $CO_2/^3He$ (3.2 × 10^{11} to 3.2 × 10^{13}) and lower helium isotope values compared RVP gas samples.

(2) three additional gas samples (all from Mampulo Spring #2) fall on the mixing line between mantle endmembers and radiogenic ^4He.
(3) the four remaining gas samples, three from the Ngozi-Songwe (Mesa and Quarry localities) and one from Kiejo-Mbaka (Kilambo Springs), plot on a trajectory extending from mantle values of ~6–8 R_A towards the CO_2 apex (i.e., high $CO_2/^3He$). This relationship is compatible with mixing between crustal and mantle endmembers.

Therefore, we conclude that there is significant mantle-derived helium, and by inference mantle CO_2, present in all RVP gas-phase samples. Notably, the six relatively unmodified (mantle-like) samples are all cold CO_2 mazuku-like vents, and thus plot close to the MORB/SCLM value in Fig. 4A. However, all additional gas samples can be explained by a mantle-like source composition, and subsequent mixing with crustal components. In Section 5.4 we use mixing models to calculate relative (%) mantle and crustal contributions.

Another feature of the RVP dataset (Fig. 4A) is the marked disparity in elemental ratios (e.g. $CO_2/^3He$) between fluid and gas-phase samples. Fluid and gas-phase $CO_2/^3He$ ratios range from ~10^9 to ~10^{13}; however, all fluid-phase samples display relatively high $CO_2/^3He$ ratios (> 10^{11}) consistent with significant elemental fractionation between the two volatile species — most likely resulting from hydrothermal degassing and/or solubility controlled phase-separation (see Section 5.2). As a result, all RVP fluid samples plot in a cluster close to the CO_2 apex. In order to identify and interpret fluid variations, a second ternary diagram, with a contracted scale, is shown (Fig. 4B). Notably, the majority of fluid-phase samples displays significantly lower $^3He/^4He$ values compared to gas-phase samples, suggesting that fluid samples contain more radiogenic (crustal) helium. Thus, we conclude that fluids are

more susceptible to radiogenic ^{4}He additions, particularly following volatile depletion induced by phase-separation. These processes are discussed in detail in Section 5.2.

We also plot the northern Tanzania samples (n = 6) in Fig. 4A and note that Oldoinyo Lengai samples (n = 2) overlap, and help define, the SCLM endmember values, plotting close to the mazuku vents. In contrast, Lake Natron waters (n = 4) display significantly lower $CO_2/^3He$ values ($<2\times10^9$) compared with RVP fluids ($>10^{11}$), indicating that a process acting to decrease $CO_2/^3He$ values has extensively modified them. In the next section, we investigate the effects of CO_2 loss due to calcite precipitation as a means to lower $CO_2/^3He$ ratios for these Lake Natron samples.

5.2. Potential fractionation processes

Phase separation within a hydrothermal system can potentially fractionate both elemental (i.e., $CO_2/^3He$) and isotope (i.e., $\delta^{13}C$) ratios. Phase-partitioning can be caused by either vapor/steam separation at high temperatures (>100 °C) and/or gas exsolution due to supersaturation of a particular gas species. In both cases, elemental fractionation can occur between CO_2 and He due to the greater solubility of CO_2 in aqueous solution relative to helium (Ellis and Golding, 1963; Weiss, 1971). Solubility experiments indicate that CO_2 is ~42 times more soluble than He in water at temperatures up to 100 °C (Ellis and Golding, 1963; Stephen and Stephen, 1963; Ozima and Podosek, 1983): therefore, helium partitions preferentially into the vapor phase relative to CO_2. As a result, gas-phase $CO_2/^3He$ ratios will represent a minimum estimate of the original (starting) ratio and fluid samples containing residual volatiles would be expected to have higher $CO_2/^3He$ values. Phase-separation can also cause isotopic fractionation as the partitioning of CO_2 between water vapor and liquid induces fractionation between $^{13}CO_2$ and $^{12}CO_2$ (Vogel et al., 1970; Mook et al., 1974; van Soest et al., 1998; Ray et al., 2009) with $^{13}CO_2$ being relatively depleted in the vapor phase at temperatures <110 °C.

Notably, the lowest $CO_2/^3He$ values from RVP are observed in cold CO_2 mazuku vents on the flanks of the Rungwe and Kiejo volcanoes, falling within error of the typical MORB $CO_2/^3He$ range (e.g., $2\pm1\times10^9$) (Marty and Jambon, 1987), whereas fluid samples extend upwards over several orders of magnitude. If we assume a mantle-like starting composition ($\sim2\times10^9$) then the absence of lower values at RVP implies that processes such as magma degassing prior to eruption and/or calcite precipitation – processes that act to lower $CO_2/^3He$ in residual volatiles (Ray et al., 2009) – cannot have a marked effect. However, we note that extensive travertine deposits are found at RVP (particularly the Songwe region) indicating that, at this locality at least, calcite precipitation may have an effect on $CO_2/^3He$ values. To further assess the potential effects of phase-separation and/or calcite precipitation on RVP fluid samples, we consider the relationship between volatile (He and CO_2) content and $CO_2/^3He$ ratios in order to identify possible links between extreme $CO_2/^3He$ values and highly degassed, low concentration fluid samples (following Van Soest et al., 1998) .

5.2.1. Effects of hydrothermal phase-separation: $CO_2/^3He$

$CO_2/^3He$ versus helium concentration $[He]_C$ (μcm^3 STP/g H_2O) for all fluid samples from RVP and northern Tanzania is plotted in Fig. 5A. Fluid samples with <0.1 $[He]_C$ μcm^3 STP/g H_2O clearly display the highest measured $CO_2/^3He$ values. Furthermore, all fluid samples display significantly higher ($>10^{11}$) $CO_2/^3He$ compared to corresponding gas-phase samples. For example, two of the four samples with >0.1 $[He]_C$ μcm^3 STP/g H_2O have corresponding gas-phase samples (collected from the same locality) with (significantly lower) $CO_2/^3He$ ratios, which fall within the MORB range.

5.2.2. Effects of calcite precipitation: $CO_2/^3He$

In Fig. 5B we plot $CO_2/^3He$ versus $[CO_2]$ content and note that the cold Kafwira Njuni (Rungwe) sample displays the lowest $[CO_2]$ content as well as the lowest $CO_2/^3He$ value at RVP. However, no clear correlation exists between these two parameters for the remaining RVP fluid samples suggesting that calcite precipitation, which should act to lower $CO_2/^3He$ in the residual water phase, is not pervasive throughout RVP. Importantly, the observation that all fluid $CO_2/^3He$ values at RVP are significantly higher than canonical mantle values indicates that phase partitioning is the likely primary process responsible for the observed $CO_2/^3He$ variations. In contrast, northern Tanzania fluid samples from Lake Natron all display low $[CO_2]$ contents together with low $CO_2/^3He$ values which lie within or below the canonical mantle range ($2\pm1\times10^9$). The only plausible mechanism to lower $CO_2/^3He$ ratios is CO_2 loss due to calcite precipitation as any additions of crustal volatiles – consistent with the low $^3He/^4He$ ratios at Lake Natron – would act to increase values.

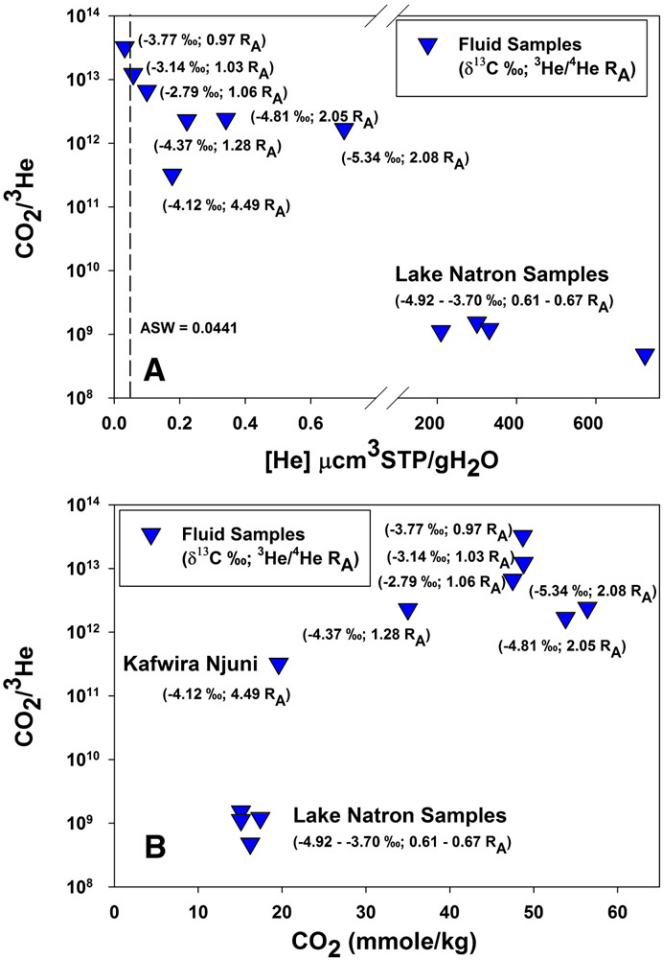

Fig. 5. A — $CO_2/^3He$ versus $[He]_C$ μcm^3 STP/g H_2O for all RVP and Lake Natron fluid samples. The three lowest [He] content samples display the highest $CO_2/^3He$ ratios. Notably, the three samples with the highest $CO_2/^3He$ values also display the three highest $\delta^{13}C$ values among RVP samples. As a result, we attribute both elemental and isotope fractionation processes at RVP to solubility controlled phase-separation within the hydrothermal system (see Section 5.2). B — $CO_2/^3He$ versus CO_2 (mmol/kg) for all RVP and Lake Natron fluid samples. The lowest $[CO_2]$ content samples are from Lake Natron and display the lowest $CO_2/^3He$ values, suggesting that CO_2 loss due to calcite precipitation may be responsible for the low $CO_2/^3He$ values observed in this region. However, there is no clear correlation between $CO_2/^3He$ and $[CO_2]$ content with the remaining RVP samples, indicating that CO_2 loss does not significantly affect RVP $CO_2/^3He$ values.

5.2.3. Fractionation effects on helium ($^3He/^4He$) and carbon isotopes ($\delta^{13}C$)

Here, we consider the effects of phase partitioning and calcite precipitation on the carbon and helium isotope systematics. We note that all fluid samples display higher carbon isotope ratios (−2.79 to −3.77‰) relative to corresponding gas-phase samples

(−5.36 to −6.45‰) collected at the same locality (Fig. 3). Moreover, the three highest measured $\delta^{13}C$ values occur in the fluid-phase of the three most extremely fractionated and helium poor samples (i.e., those with the highest $CO_2/^3He$ and lowest $[He]_C$ μcm^3 STP/g H_2O) (Fig. 5A). These $\delta^{13}C$ variations are consistent with experimentally-determined isotopic ($^{13}C/^{12}C$) fractionation factors at low (<60 °C) temperatures, with ^{13}C being relatively depleted in the vapor phase (Vogel et al., 1970). At temperatures up to ~110 °C, the C isotope fractionation factor between vapor and liquid is greater than unity (i.e. $(\alpha^{13}C_{vapor-liquid} > 1)$ (Mook et al., 1974; Zhang et al., 1995; Szaran, 1997): all RVP samples have discharge temperatures below this temperature-threshold and display $\delta^{13}C$ values consistent with phase separation within the hydrothermal system.

Finally, we note that fluid-phase samples generally display lower He-isotope ratios relative to gas-phase samples. For example, at the three localities where both fluid and gas-phases samples were collected, two of the three fluid-phase samples (e.g., Songwe and Kilambo Springs) displayed significantly lower $^3He/^4He$ ratios versus the corresponding gas-phase sample, with the third sample (i.e., Mampulo Spring) displaying overlapping $^3He/^4He$ values between the two phases. Furthermore, we note that Songwe and Kilambo Springs are among the most volatile depleted (i.e., He-poor) fluid samples whereas the Mampulo Spring samples are the most volatile enriched RVP fluid samples. Therefore, we suggest that lower $^3He/^4He$ ratios are observed in fluid-phase samples because they are more susceptible to record radiogenic (crustal) additions of helium due to lower volatile concentrations following phase-separation. If a significant portion of the intrinsic magmatic volatile signature is lost to the vapor phase, small additions of radiogenic ^4He can drastically reduce the $^3He/^4He$ ratio of any He residual in the water phase.

In summary, the effect of hydrothermal phase-separation has significantly altered the He–CO_2 characteristics of all fluid-phase samples, resulting in extremely high $CO_2/^3He$ values ($>3\times10^{11}$) due to preferential helium loss from the fluid-phase. Therefore, gas-phase samples are considered most representative of magmatic sources at RVP, and are thus able to provide greater insight into primary mantle source characteristics.

5.3. Crustal-mantle mixing

In this section, we use both gas and fluid phase results to illustrate the effects of crust–mantle mixing on the He isotope systematics and to further demonstrate that gas phase samples possess the most representative signature of the mantle source. We consider a variety of factors, such as proximity to volcanic center, elevation and temperature constraints, which may act individually or together to control the extent of crust–mantle interaction.

5.3.1. Crustal–mantle mixing: proximity to volcanic center

In Fig. 6 we plot sample temperature and sampling locality elevation as well as distance from the nearest volcanic edifice versus the helium isotope ($^3He/^4He$) composition. The highest proportions of magmatic volatiles (i.e., highest $^3He/^4He$ ratios) are found at the cold CO_2 mazuku vents (Fig. 6A), on the flanks of Kiejo and Rungwe volcanoes, with $^3He/^4He$ ratios systematically decreasing with increasing distance from the volcanic edifice ($R^2 = 0.68$) (Fig. 6C). Similar spatial patterns of $^3He/^4He$ versus distance from volcano summits have been reported previously for hydrothermal fluids at volcanoes worldwide (e.g., Sano et al., 1984; Marty et al., 1989; Hilton et al., 1993; Van Soest et al., 1998). These results suggest that high elevation cold mazuku vents (Fig. 6B), collected relatively close to the summits (<11 km), derive their volatiles from a MORB-like or SCLM source and that they have remained unmodified by extraneous volatile additions. In contrast, more distally-located hydrothermal samples from both Ngozi-Songwe and Kiejo-Mbaka hydrothermal systems have been affected by additions of radiogenic He (Fig. 4A), likely due to more extensive interaction with ^4He-rich basement rock during deep circulation of fluids in the hydrothermal system.

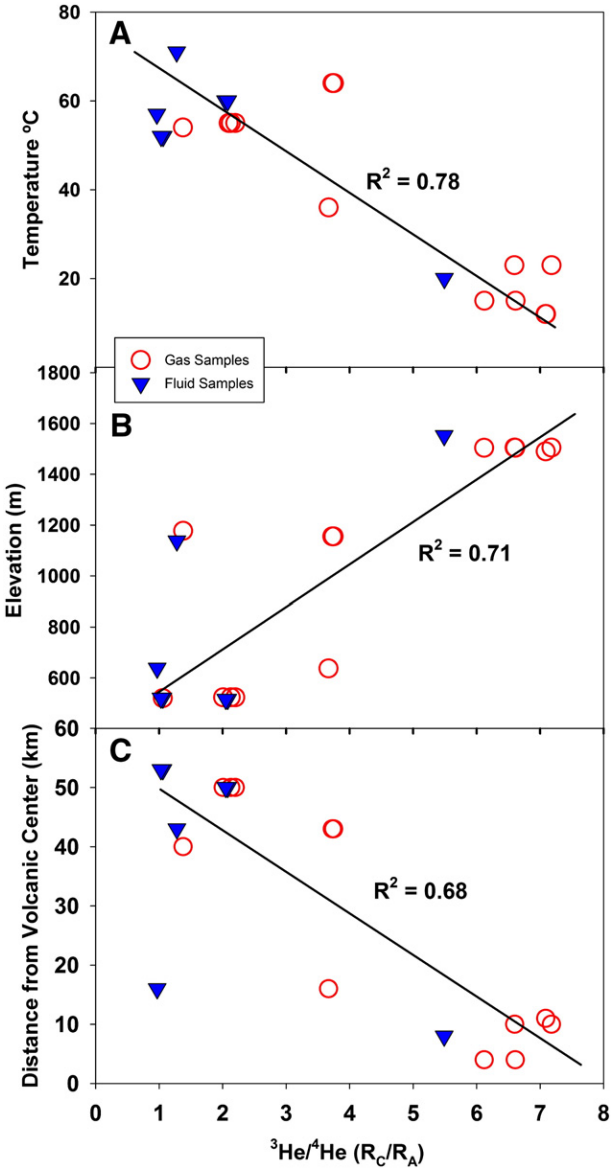

Fig. 6. He-isotopes versus distance from volcanic edifice (km) (6A), elevation (m) (6B), and temperature (°C) (6C) for fluid (blue triangles) and gas (red open circles) samples of RVP. Both fluid and gas phase samples are considered as He-isotopes are not affected by modification processes such as phase separation. Notably the highest measured (MORB-like) $^3He/^4He$ ratios are from the highest elevation and lowest temperature CO2 mazuku vent samples found in close proximity to volcanic centers.

5.3.2. Crustal–mantle mixing: temperature-helium isotope relationships

The most pristine, mantle-like, $^3He/^4He$ values at RVP occur in the low temperature CO_2 mazuku gas vents (Fig. 6A) found in close proximity to topographic highs on the flanks of Rungwe and Kiejo volcanoes (Fig. 6B). Indeed, the coldest gas sample of this study (Kibila Cold Vent; T = 12 °C) has the second highest $^3He/^4He$ value (7.09 R_A). This observation can be contrasted with the Songwe Overlook sample which is the hottest fluid sampled (T = 71 °C) yet possess one of the lowest $^3He/^4He$ values measured in this study. Surprisingly, therefore, the highest $^3He/^4He$ samples are associated with the lowest sample temperatures (12–23 °C) — in some cases, lower than ambient air temperatures.

In general, the occurrence of magmatic helium in high enthalpy hydrothermal samples implies a direct transfer of heat and helium between magmatic and hydrothermal systems (e.g., Torgersen and Jenkins, 1982). In the case of RVP, however, the temperature-helium relationships indicate that heat and (magmatic) volatile transfer are apparently inversely related and potentially decoupled. Indeed, the lowest temperature (mazuku) samples have the highest $^3He/^4He$ values. We suggest two hypotheses to explain this observation:

(1) Low temperatures in gas-phase samples result from a combination of geothermal gradient cooling at higher elevations (~18.3 °C/km) (Tiab and Donaldson, 2011), conductive cooling associated with colder meteoric-water recharge temperatures at higher elevations (Delalande et al., 2011; de Moor et al., 2013-this issue), and possibly adiabatic expansion and rapid cooling of gases during release to the surface. Adiabatic cooling is supported by our field observation that the coldest (~12 °C) mazuku gases (Kibila Cold Vent) display the most vigorous degassing rates. A combination of these three processes near volcanic centers could act to transfer relatively unmodified magmatic volatiles to surface manifestations while effectively dampening corresponding heat transfer.

(2) Alternatively, low temperature gas-phase (mazuku) vents are completely decoupled from the hydrothermal systems at RVP and thus are immune from modifications associated with volatiles derived from the hydrothermal system. Mazuku form as gases accumulate in cavities or partially-drained lava flow tunnels following eruptive events (Smets et al., 2010). As a result, pristine mantle-derived volatiles could accumulate in large cavities during prior eruptive events, only to be subsequently released at lava flow contacts or by recent faulting. All mazuku vents were collected at stratigraphic contacts between phonolitic tuff units and basalts (Harkin, 1960; see also Tedesco et al., 2010). This volatile storage and release mechanism could explain (a) low discharge temperatures (as isolated gases would have ample time to cool), (b) the rarity of mazuku, (c) their restricted occurrence — only along volcanic flanks and at lava flow contacts, and (d) the pristine nature of these gases.

In contrast, we propose that higher temperatures (50–70 °C) and associated low He-isotope ratios are related to conductive heat transfer associated with faulting and (deep) infiltration and circulation of hydrothermal fluids (de Moor et al., 2013-this issue) during transport through ^4He-rich country rocks (Section 5.3.1). The negative correlation between temperature and $^3He/^4He$ (Fig. 6A) indicates that high temperatures may promote leaching and facilitate release of radiogenic ^4He from water-bearing reservoir rocks (Porcelli and Ballentine, 2002). Mantle volatiles are ubiquitous throughout RVP, so increased travel times with increasing distance from volcanic centers would act to mask magmatic $^3He/^4He$ ratios with greater contributions of radiogenic He (Fig. 6C).

5.4. RVP volatile provenance (% mantle and crust)

In this section, we calculate relative mantle and crustal contributions to the volatile inventory using He and combined He–CO_2 systematics.

5.4.1. Helium isotope mixing model

Utilizing only representative non-fractionated gas-phase samples (see Section 5.2), we first calculate mantle He contributions by assuming He-isotope distributions at RVP are controlled by simple two-component mixing between radiogenic helium (derived from ^4He-rich country rocks) and mantle-derived helium. We consider three mixing scenarios, each with different mantle endmembers (e.g., High $^3He/^4He$, MORB, SCLM). In the 'High $^3He/^4He$ endmember' case, samples are divided according to hydrothermal system (Fig. 1B), and assigned a He endmember value based on the highest measured phenocryst $^3He/^4He$ value from the nearest volcanic center (e.g., Ngozi-Songwe = 14.9 R_A, Rungwe = 12.2 R_A, Kiejo = 10.3 R_A; Hilton et al., 2011) associated with a particular hydrothermal system. In Table 2, we compare these results to endmember scenarios calculated with upper-mantle He endmembers: MORB = 8 R_A and SCLM = 6.1 R_A (Graham, 2002; Gautheron and Moreira, 2002). If a 'High $^3He/^4He$' endmember is used then the He-isotope distributions of the most pristine gases (e.g., Kiejo Cold Vent, Kibila Cold Vent and Ikama Village samples) can be explained by 54–64% mantle contributions. In contrast, when a MORB-like He-isotope endmember is evoked, these same samples involve 76–90% mantle contributions versus 100% mantle contribution if a SCLM-like He-isotope endmember is selected. Importantly, if an upper-mantle (MORB, SCLM) He-isotope endmember is adopted, these data suggest that virtually pristine unmodified mantle gases are vigorously degassing

Table 2
Proportions of mantle versus crustal helium and mantle versus limestone versus sediment derived carbon contribution to each sample.

Sample location	Phase[a]	Proportion of High $^3He/^4He$ He (%) [b]	Proportion of MORB He (%) [c]	Proportion of SCLM He (%) [d]	(CO_2 %) [e] mantle	(CO_2 %) [e] limestone	(CO_2 %) [e] sediments
Rungwe Volcanic Province (RVP)							
Ngozi-Songwe hydrothermal system							
Songwe Mesa	G	24.8	46.3	60.8	5.6	77.7	16.7
(Dup)	G	24.9	46.5	61.2	8.8	72.8	18.4
Songwe Quarry	G	9.0	16.7	22.0	0.1	80.2	19.7
Kiejo-Mbaka hydrothermal system							
Kilambo Springs	G	35.3	45.5	59.8	3.4	79.2	17.4
Mampulo Spring #2	G	17.7	27.0	35.5	65.6	27.1	7.3
(Dup)	G	17.1	26.2	34.4	68.0	26.7	5.3
(Dup)	G	16.1	24.7	32.4	62.3	29.8	7.9
Cold CO_2 mazuku vents							
Ikama Village	G	53.9	82.4	100	44.1	50.2	5.6
(Dup)	G	58.7	89.7	100	44.8	47.7	7.5
Kibila Cold Vent	G	57.9	88.6	100	50.0	46.7	3.3
(Dup)	G	57.9	88.6	100	44.1	52.5	3.4
Kiejo Cold Vent	G	59.2	76.4	100	51.9	44.6	3.5
(Dup)	G	64.0	82.5	100	37.4	54.1	8.4

[a] Sample phase: G = gas.
[b] Considering a simple binary mixture between "High $^3He/^4He$" (Ngozi-Songwe = 14.9 R_A, Rungwe = 12.2 R_A, Kiejo = 10.3 R_A) and crustal helium (0.05 R_A).
[c] Considering a simple binary mixture between MORB (8 R_A) and crustal helium (0.05 R_A).
[d] Considering a simple binary mixture between SCLM (6.1 R_A) and crustal helium (0.05 R_A).
[e] Assuming $\delta^{13}C$ values of −6.5‰, 0‰ and −30‰ (relative to VPDB) with corresponding $CO_2/^3He$ ratios of 2×10^9, 1×10^{13} and 1×10^{13} for mantle, limestone and sediments.

from low temperature mazuku gas vents at the Kiejo Cold Vent, Kibila Cold Vent and Ikama Village.

5.4.2. $CO_2/^3He$–$\delta^{13}C$ mixing model

In order to determine relative CO_2 contributions from potential endmembers at RVP, we plot $CO_2/^3He$ ratios versus $\delta^{13}C$ for the gas phase samples (Fig. 7). Potential endmembers contributing to the CO_2 inventory are mantle (M), limestone (L) and sediment (S), and assumed endmember compositions are: $\delta^{13}C = -6.5‰$ for (M), 0‰ for (L), −30‰ for (S) (relative to VPDB), and $CO_2/^3He = 2\times10^9$ for (M), 10^{13} for (L) and (S) (Sano and Marty, 1995). Superimposed on the diagram are the trajectories for binary mixing between (1) M and L, (2) M and S, and (3) L and S. The most important feature of Fig. 7 is that all samples plot within the area bounded by the three mixing trajectories, indicating that gas samples require a contribution from all three endmembers to explain their combined $CO_2/^3He$–$\delta^{13}C$ characteristics.

In Table 2 we provide a quantitative estimation of the various contributions of the three endmembers to the total carbon inventory at RVP. In the Kiejo-Mbaka system, mantle and limestone-derived carbon are the principal contributors to the carbon budget in all cases, typically representing >90% of the total. The highest mantle CO_2 contributions (62–68%) were measured in Mampulo Spring in an area marked by relatively low $^3He/^4He$ values (2.01–2.20 R_A). Sedimentary organic carbon is a minor contributor to all but one sample (Kilambo Springs; 17%). The finding that limestone contributions are more significant than organic contributions is consistent with widespread travertine deposition throughout the region (Hochstein et al., 2000). In contrast, the Ngozi-Songwe system displays the highest limestone contributions, where samples were collected at or adjacent to a travertine quarry. Notably this area is also marked by the highest organic carbon contributions and the lowest (<10%) mantle contributions. The cold CO_2 mazuku vents are characterized by 37–51% mantle-derived CO_2, with mantle and limestone-derived carbon comprising >90% of the total for all samples. Note, however, if a SCLM $CO_2/^3He$ endmember value of 4×10^9 is adopted (see Section 5.1), the proportion of mantle-derived CO_2 of the mazuku increases to >90%. In effect, virtually the entire He and CO_2 inventory is derived from the mantle.

5.4.3. He–CO_2 crustal–mantle endmember contributions

In addition to quantifying the relative proportions of mantle and crustal contributions to the He–CO_2 volatile inventory, we can also ascertain the relative roles of the crustal and mantle endmembers in supplying the CO_2. In Fig. 8, we plot $^3He/^4He$ versus $CO_2/^3He$ with binary mixing trajectories between a MORB like starting composition and various crustal $CO_2/^3He$ endmembers (1×10^9–1×10^{15}). We note that: (1) all but one gas-phase sample (Songwe Quarry) can be explained by binary mixing between a mantle (MORB-like) endmember and a crustal-$CO_2/^3He$ endmember in the range between ~1×10^{11} and 5×10^{13}, and (2) nine of thirteen gas-phase samples fall on a mixing trajectory between MORB and a crustal $CO_2/^3He$ endmember of ~10^{13}. By adopting these endmembers, all six mazuku samples plot in a cluster close to the mantle endmember, indicating a minimal (5–10%) contribution of the crustal endmember ($CO_2/^3He = 10^{13}$) in supplying the CO_2. The three remaining samples (e.g., Kilambo Springs and duplicate samples from Songwe Mesa) display higher $CO_2/^3He$ and are characterized by larger contributions (42–68%) of the crustal endmember ($CO_2/^3He = 10^{13}$). The observation that 9 of 13 gas phase $CO_2/^3He$ values can be explained by mixing between MORB ($CO_2/^3He = 2\times10^9$) and a crustal endmember with $CO_2/^3He = 10^{13}$ confirms that assumed (L) and (S) $CO_2/^3He$ values used to calculate CO_2 provenance (above) are justified (see Table 2; Fig. 7). However, four RVP samples (i.e., Mampulo #2 and duplicates and Songwe Quarry) require different crustal $CO_2/^3He$ endmember values to explain their combined $^3He/^4He$ and $CO_2/^3He$ characteristics. This indicates that the RVP crust is heterogeneous with respect to $CO_2/^3He$, likely resulting from variable crustal compositions. For example, if present, old basaltic lithologies would impart mantle-like $CO_2/^3He$ values (~2×10^9) whereas sediments (organic and/or limestone) would typically display much higher $CO_2/^3He$ values (~10^{13}) — see Fig. 8.

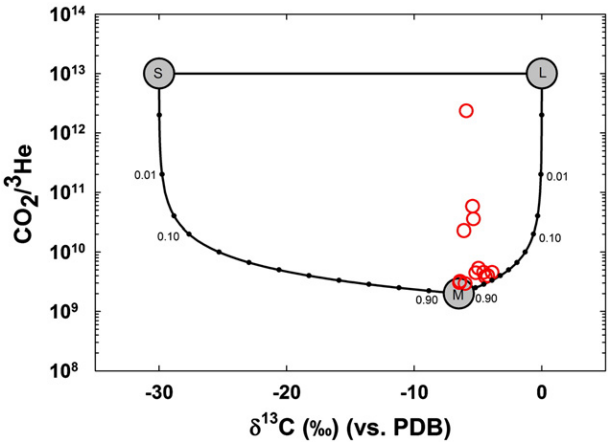

Fig. 7. Plot of $CO_2/^3He$ versus $\delta^{13}C$ for RVP gas samples. The endmember compositions for sedimentary organic carbon (S), mantle carbon (M) and limestone (L) are $\delta^{13}C = -30$, −6.5 and 0 ‰; and $CO_2/^3He = 1\times10^{13}$, 2×10^9 and 1×10^{13}, respectively (Sano and Marty, 1995). In addition, mixing trajectories between the various components are shown with fractions of the mantle contribution. Note: all data can be explained by a 3-component mixing model between M–L–S.

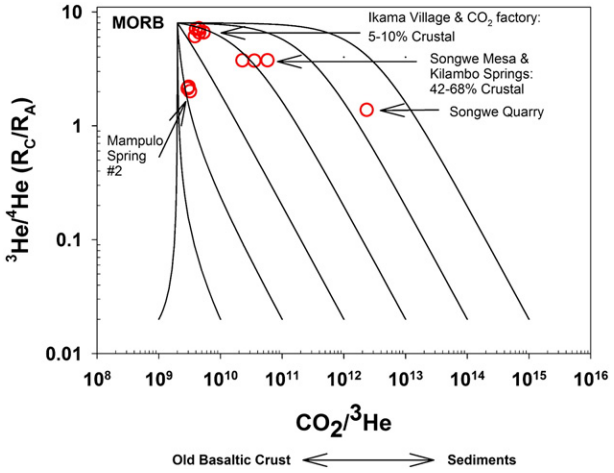

Fig. 8. $CO_2/^3He$ versus He-isotopes with mixing trajectories between a MORB-like starting composition and various crustal $CO_2/^3He$ endmembers (1×10^9–1×10^{15}). Note: all data can be explained by mixing relationships between a mantle endmember and a crustal endmember between 1×10^{11} and 5×10^{13} with the exception of one (Ngozi-Songwe) sample that indicates a mixing trajectory between a mantle endmember and a $CO_2/^3He$ value of ~5×10^{15}.

5.5. CO_2 flux calculations

By combining measured fluid CO_2 contents (TDIC) with estimated regional fluid discharge rates (Hochstein et al., 2000), a first order estimate of the CO_2 and ^3He fluxes from the two hydrothermal systems of RVP and the Lake Natron region of northern Tanzania can be estimated. Using these results, and previously published heat loss estimates from the respective regions (Hochstein et al., 2000), we also estimate the ^3He/enthalpy relationships for comparison with other hydrothermal systems worldwide (see Table 3).

The fluid discharge rate for the Ngozi-Songwe hydrothermal system is estimated to be between 50 and 70 l/s (Hochstein et al., 2000), with a median temperature of 60 °C, this leads to a total heat transfer of 10 MW (Hochstein et al., 2000). Assuming that our measured CO_2

Table 3
Helium and carbon fluxes of fluids from RVP and northern Tanzania.

Sample location	Discharge temp. (°C)	Heat Output (MW)[a]	$^3He/^4He$ (R_C/R_A)	$CO_2/^3He$ ($\times10^9$)	$[CO_2]$ (mmol/kg)	Fluid discharge (l/s)[a]	Total CO_2 flux ($\times10^7$mol/yr)	Total ^3He flux ($\times10^{-5}$ mol/yr)	^3He/enthalpy ($\times10^{-15}$ mol/J)
Rungwe Volcanic Province (RVP)									
Ngozi-Songwe hydrothermal system									
Songwe Overlook	71	10	1.28	2300	35.0	50–70	6–8	2–4	2–3
Kiejo-Mbaka hydrothermal system									
Kilambo Springs	57	3.5–7.0	0.97	32,200	48.7	20–40	3–6	0.1–0.2	0.2
Mampulo & Kasimulo Springs	56*	1.0	1.56*	5740*	51.6*	5–10	1–2	0.1–0.3	1–2
Northern Tanzania (Lengai/Lake Natron)									
Lake Natron	51*	50	0.64*	1.09*	15.9*	~1000	50	46,000	6600
Reference values									
Lower Mantle[b]	–	–	–	–	–	–	–	–	24,000
Upper Mantle[b]	–	–	–	–	–	–	–	–	500
Hydrothermal Vent (Mid Atlantic Ridge)[c]	–	–	–	–	–	–	–	–	130
Hydrothermal Vent (Galapagos Rift)[d]	–	–	–	–	–	–	–	–	120
Hydrothermal Vent (Juan de Fuca Ridge)[d]	–	–	–	–	–	–	–	–	120
Young Volcanoes (Krafla, Iceland)[e]	–	–	–	–	–	–	–	–	14,000
Cooling Lavas (Hveragaerdi, Iceland)[e]									15
Western Anatolia (Turkey)[f]	–	–	–	–	–	–	–	–	190

*Average value — calculated as mean of all samples at the locality.
[a] Values taken from Hochstein et al. (2000).
[b] Values taken from Elderfield and Schultz (1996).
[c] Values taken from Rudnicki and Elderfield (1992).
[d] Values taken from Lupton et al. (1989).
[e] Values taken from Poreda and Arnórsson (1992).
[f] Values taken from Mutlu et al. (2008).

concentration of 35 mmol/kg (Songwe Overlook) is representative of the system then the total CO_2 flux from Songwe is ~$6–8\times10^7$ mol/yr. In the Kiejo-Mbaka hydrothermal system, discharge rates (20–40 l/s; Hochstein et al., 2000) have been estimated for Kilambo Springs so that the CO_2 flux from this area is ~$3–6\times10^7$ mol/yr assuming a CO_2 concentration of 49 mmol/kg (Table 1). In the Mampulo and Kasimulo Springs area, near Lake Malawi in the south, the fluid discharge rate is estimated to be significantly lower (5–10 l/s; Hochstein et al., 2000) and as a result the CO_2 flux from this area is just ~$1–2\times10^7$ mol/yr for an assumed CO_2 concentration of ~50 mmol/kg. Given that these localities dominate the fluid flux at RVP (Hochstein et al., 2000) then our best estimate of the total flux of CO_2 transferred to the surface dissolved in hydrothermal fluids for RVP is 9–16 ($\times10^7$ mol/yr). Using the estimated contributions of the mantle endmembers to the total CO_2 inventory allows an estimate of the mantle-derived flux of CO_2 to the surface. At Ngozi-Songwe, we estimate the mantle CO_2 contribution to be ~7% using the Songwe Mesa locality: at Kiejo-Mbaka, we estimate mantle contributions to be ~3% (Kilambo Springs locality) and ~65% at the Mampulo Spring locality. Combining these percentage contributions (Table 2) with the total CO_2 fluxes from each area (Table 3), we estimate a total mantle-derived CO_2 flux of 1.0–1.9 ($\times10^7$ mol/yr) for RVP. Furthermore, we note that this estimate does not include gas phase emissions nor CO_2 released via mazuku vents (see de Moor et al., 2013-this issue) and consequently represents a minimum estimate only.

In contrast, the Lake Natron region in northern Tanzania has a much higher fluid discharge rate of ~1000 l/s (Hochstein et al., 2000) resulting in a higher total CO_2 flux of ~50×10^7 mol/yr. However, the mantle-derived CO_2 component most likely represents only a minor proportion of the total CO_2 given the low $^3He/^4He$ ratios at this locality. Furthermore, a substantial fraction of the total CO_2 has been sequestered (Section 5.2.2) resulting in low measured $CO_2/^3He$ ratios. Therefore, the mantle CO_2 flux is unknown at Natron but likely represents a small fraction of the estimated total CO_2 flux. Notably, taken together, the mantle CO_2 fluxes at Lake Natron and RVP represent a negligible fraction of the global ridge CO_2 flux (~2.2×10^{12} mol/yr) (Marty and Tolstikhin, 1998).

By combining CO_2 flux estimates with measured $CO_2/^3He$ values, ^3He fluxes of $2–4\times10^{-5}$ mol/yr, $0.1–0.2\times10^{-5}$ mol/yr, $0.1–0.3\times10^{-5}$ mol/yr and $46{,}000\times10^{-5}$ mol/yr are calculated for Songwe, Kilambo, Mampulo and Kasimulo and Lake Natron, respectively (Table 3). These fluxes are combined with heat loss estimates (Hochstein et al., 2000) to calculate ^3He/enthalpy ratios — which are believed to be controlled by the maturity of the magmatic system (Poreda and Arnórsson, 1992). ^3He/enthalpy estimates are orders of magnitude higher in the Lake Natron (6600) region compared to RVP (~5), suggesting a significantly more active system. For comparison, we provide ^3He/enthalpy estimates from other regions, including recently-active (Krafla) and cooling magmatic systems (Hveragaerdi) of Iceland (Table 3). We note that RVP ^3He/enthalpy values are similar to cooling magma systems at Hveragaerdi whereas Lake Natron values are much closer to ratios expected at active volcanic centers. These results are not surprising considering the dormant nature of RVP volcanic centers and the highly active nature of Oldoinyo Lengai volcano, found in close proximity to Lake Natron.

5.6. Gas and fluid phase versus lava $^3He/^4He$: apparent He-isotope discrepancy

In subaerial plume-driven rift zones, such as Afar and Iceland, there is generally good correspondence between $^3He/^4He$ values in hydrothermal fluids and mafic mineral phases such as olivine and pyroxene suggesting that these various sample media are capturing He from the same mantle source(s) (Hilton et al., 1990; Scarsi and Craig, 1996; Marty et al., 1996; Füri et al., 2010). However, Hilton et al. (2011) made the observation that RVP hydrothermal fluid $^3He/^4He$ values (~1–7 R_A) (Pik et al., 2006) do not significantly overlap with $^3He/^4He$ values (~7–15 R_A) in mineral separate samples. The results of this study (Table 1) confirm this apparent He-isotope discrepancy with the most pristine gas-phase (mazuku) samples from RVP lying in the SCLM to MORB range, suggesting no involvement of (plume-like) mantle in supplying He to the region. This observation is illustrated in Fig. 9A which plots $^3He/^4He$ ratios in fluids/gases versus mafic crystals (olivine and clinopyroxene). In this section, we investigate factors that could potentially control this apparent He-isotope discrepancy by addressing the following queries: (1) Is this He-isotope discrepancy real, or simply the result of restricted/

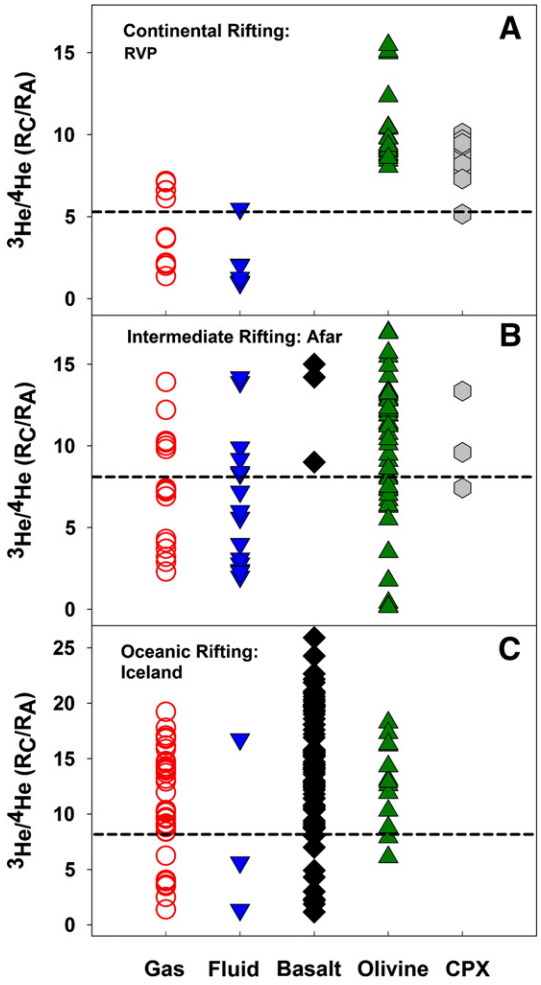

Fig. 9. Helium isotopes measured in different sample phases (gas, fluid, basalt, olivine and clinopyroxene) from three distinct plume-related subaerial rift systems. Fig. 9A illustrates the apparent He-isotope disparity between hydrothermal fluids and gases (this study) and phenocrysts (Hilton et al., 2011) values at RVP. In contrast, at intermediate rift zones (e.g., Afar; Main Ethiopian Rift — Fig. 9B) (Scarsi and Craig, 1996; Marty et al., 1996) and oceanic spreading centers (e.g., Iceland — Fig. 9C) (Füri et al., 2010) there is significant overlap between hydrothermal and rock derived samples.

limited hydrothermal sampling opportunities at RVP? (2) Could this discrepancy be the result of temporal He-isotope variations? (3) Are variations in rift dynamics, such as extent of lithospheric extension, crustal thickness and crustal age, influencing the degree of crustal modification and hence preferentially lowering $^3He/^4He$ in some sample types?

The primary finding of this study is that pristine SCLM to MORB-like mantle $^3He/^4He$ values (~7 R_A) are found at three distinct sites (Kiejo Cold Vent, Kibila Cold Vent and Ikama Village), and that these localities are characterized by vigorously degassing cold CO_2 (mazuku-like) vents in close proximity to volcanic edifices. In contrast, predominantly mantle-like $^3He/^4He$ ratios (i.e. $^3He/^4He > 7$ R_A; n = 30) were measured in mafic phenocrysts throughout RVP (Hilton et al., 2011), with 14 values falling in the MORB range (8 ± 1 R_A), (b) 9 lying between 9 and 10 R_A and (c) 7 falling above 10 R_A. Notably, phenocryst samples closest to Ikama Village (i.e., within 1 km; samples RNG-8, 9, 11, 12) have an average $^3He/^4He$ value of 8.7 R_A, with the closest (~8 km) sample to Kiejo Cold Vent (TAZ09-12) also yielding a $^3He/^4He$ value of 8.7 R_A (Hilton et al., 2011). On a spatial basis, therefore, there is not a $^3He/^4He$ disparity between phenocrysts and geothermal fluids/gases as both capture MORB-like He. In this respect, we could argue that the absence of hydrothermal samples and/or mazuku in close proximity to high (plume-like) $^3He/^4He$ phenocryst localities could explain why plume-like $^3He/^4He$ ratios (>10 R_A) are not found in fluid and gas samples. A more comprehensive sampling strategy would enable us to test this suggestion further.

Regarding the possibility that there is a temporal control on the presence of (plume-like) $^3He/^4He$ ratios at RVP, we note the observation that high $^3He/^4He$ values are found in both Younger and Older Extrusive rocks (Hilton et al., 2011) suggesting that the high $^3He/^4He$ component is a long-term, as opposed to transient or ephemeral, feature of the underlying mantle source. As a result, plume-like He should potentially be detectable in present-day hydrothermal activity. Its absence, therefore, points to another factor — in addition to the proximity issue discussed above, as the reason why high $^3He/^4He$ ratios are not found in fluids and gases.

We suggest that the likeliest scenario to explain lower $^3He/^4He$ values in hydrothermal fluids involves large-scale tectonic factors such as plume–craton interaction and the introduction of radiogenic He into the gas/fluid phases. This case is made based upon a comparison between three different subaerial plume-driven rift zones: RVP, Afar, and Iceland, all at various stages of development and characterized by different crustal thicknesses. In the first case, RVP is a nascent continental rift zone located at the southern terminus of the EARS, within Precambrian orogenic belts, on the margin of the Tanzanian Craton — itself comprised of Archean (3.0–2.6 Ga) amalgamated terrains (Maboko, 2000; Manya et al., 2006; Yirgu et al., 2006; Furman, 2007). Furthermore, geophysical and xenolith evidence suggest that the Tanzanian craton has a deep (200–350 km) lithospheric keel that has not been extensively disrupted by Cenozoic tectonic and/or magmatic activity (Chesley et al., 1999; Lee and Rudnick, 1999; Ritsema et al., 1999; Belluci et al., 2011). As a result, RVP marks the intersection of old/thick cratonic crust with contemporary plume-influenced volcanism and recent rifting. Second, the Afar region marks the northern terminus of EARS rifting and is characterized by intermediate crustal thicknesses — from ~45 km in the highlands to as thin as ~16 km in the incipient ocean spreading centers of northern Afar (Yirgu et al., 2006). Voluminous igneous crust is actively being generated and basaltic rocks are characterized by high $^3He/(U–Th)$ contents (Marty et al., 1996). Finally, Iceland is a plume-driven oceanic spreading center, marked by extremely young crust (0–17 Ma) (McDougall et al., 1984; Einarsson, 2008). Crustal thicknesses vary between 20 and 100 km, with an average rift zone age of (<2 Ma) and thickness of 20–40 km (Bjarnason et al., 1993; Bjarnason and Schmeling, 2009; Staples et al., 1997).

In Fig. 9 we plot $^3He/^4He$ values measured in hydrothermal gases and fluids, basalts, and mafic phenocryst phases (olivine and clinopyroxene) for the three different plume-driven rift zones: RVP, Afar and Iceland. We note the readily apparent He-isotope discrepancy between hydrothermal fluids and gases and mazuku versus mineral phases at RVP, compared with the considerable overlap between the various sample phases at both Afar and Iceland. Thus, we suggest that rift dynamics may control $^3He/^4He$ ratios in fluids/gases through increased interaction with ^4He derived from the crust. For example, volatiles emanating from the magmatic source at depth at RVP are exposed to old (Archean) bedrock and ^4He-rich sediments en route to the surface. Due to the relative thickness of the crust, magmatic volatiles likely undergo longer storage times, with increased potential to acquire a more radiogenic signature during ascent. In contrast, Afar crust is significantly thinner (e.g., no plume–craton interaction) so that residence times of He in various hydrothermal systems are likely reduced, along with the potential for extensive radiogenic-He additions. Similarly, radiogenic He contributions also occur in parts of the Icelandic crust (Condomines et al., 1983); however, they are generally less pervasive and typically have little effect on either hydrothermal and basalt phases (Hilton et al., 1990). Thus, it is the combination of old Archean/Proterozoic basement rocks and their derivatives that make up the fluid reservoir host rocks that imparts such a strong

radiogenic ^{4}He signal at RVP which is difficult to by-pass by most hydrothermal samples except in relatively rare cases, such as when mazuku are present.

6. Concluding remarks

This study has shown that RVP fluids and gases are characterized by a wide range of ^{3}He/^{4}He and $CO_2/^3$He vales, and a narrow range in δ^{13}C (CO_2) values, reflecting variable mantle and crustal contributions. We show that phase-separation within the hydrothermal system has a clear influence on fluid-phase samples and is likely the principal controls on their $CO_2/^3$He ratios and δ^{13}C values. Additionally, fluid samples are especially susceptible to radiogenic helium additions following gas (helium) loss and subsequent ^{4}He addition due to prolonged interaction with the crust during fluid transport.

Several cold CO_2 mazuku gas vents display He–CO_2 characteristics typical of either MORB or SCLM. Additionally, their low temperatures, rarity, and occurrence at stratigraphic contacts, together suggest that they may be derived from an isolated source that is decoupled from the modern hydrothermal system. Using He-isotope compositions, we calculate the percentage of mantle contribution to each gas-phase RVP sample for three different endmember ^{3}He/^{4}He scenarios (SCLM, MORB and 'High-^{3}He/^{4}He'). In addition, we use a $CO_2/^3$He–δ^{13}C model to quantitatively assess mantle and crustal CO_2 budgets and calculate CO_2 fluxes for fluid samples. We suggest that the extent of crustal contamination in samples is regionally controlled by proximity to volcanic edifices and extent of hydrothermal interaction; however, rift zone evolution (e.g., stage of rifting) also heavily influences observed regional trends as it acts to control the extent of ^{4}He addition from old, He-rich reservoir rocks. We conclude that the apparent He-isotope disparity between mafic phenocrysts and hydrothermal fluids does not exist on small spatial scales and that the absence of hydrothermal manifestations and/or mazuku-like features in close proximity to high ^{3}He/^{4}He phenocryst localities can explain this apparent He-isotope disparity at RVP.

Acknowledgements

We acknowledge the National Science Foundation (NSF), Earth Science Division for providing funding (EAR-1019489) to DRH. The manuscript was completed under a UC President's Dissertation Year Fellowship awarded to PHB. Field expenses for the 2009 expedition were provided by funds from the Fluids and Volatiles Laboratory (DRH) and NSF (Petrology & Geochemistry — EAR-0827352) to TPF. Discussion with Sæmundur Halldórsson and James Day as well as comments by two anonymous reviewers is gratefully acknowledged.

References

Adams, A., Nyblade, A., Weerarantne, D., 2012. Upper mantle shear wave velocity structure beneath the East African plateau: evidence for a deep, plateau wide low velocity anomaly. Geophysical Journal International 189, 123–142. http://dx.doi.org/10.1111/j.1365-246X.2012.05373.x.

Arnórsson, S., 2000. Isotopic and Chemical Techniques in Geothermal Exploration, Development and Use: Sampling Methods, Data Handling. Interpretation. IAEA, Vienna, p. 351.

Belluci, J.J., McDonough, W.F., Rudnick, R.L., 2011. Thermal history and origin of the Tanzanian Craton from Pb isotope thermochronology of feldspars from lower crustal xenoliths. Earth and Planetary Science Letters 301, 493–501. http://dx.doi.org/10.1016/j.epsl.2010.11.031.

Bjarnason, I.T., Schmeling, H., 2009. The lithosphere and asthenosphere of the Iceland hotspot from surface waves. Geophysical Journal International 178, 394–418. http://dx.doi.org/10.1111/j.1365-246X.2009.04155.x.

Bjarnason, I., Menke, W., Flovenz, O., Caress, D., 1993. Tomographic image of the spreading center in south Iceland. Journal of Geophysical Research 98, 6607–6622.

Branchu, P., Bergonzini, L., Delvaux, D., De Batist, M., Golubev, V., Benedetti, M., Klerkx, J., 2005. Tectonic, climatic and hydrothermal control on sedimentation and water chemistry of northern Lake Malawi (Nyasa), Tanzania. Journal of African Earth Sciences 43, 433–446. http://dx.doi.org/10.1016/j.jafrearsci.2005.09.004.

Burke, K., 1996. The African Plate, South Afr. Journal of Geology 99, 339–409.

Chakrabarti, R., Basu, A.R., Santo, A.P., Tedesco, D., Vaselli, O., 2009. Isotopic and geochemical evidence for a heterogeneous mantle plume origin of the Virunga volcanics, Western rift, East African Rift system. Chemical Geology 259, 273–289.

Chesley, J.T., Rudnick, R.L., Lee, C.T., 1999. Re–Os systematics of mantle xenoliths from the East African Rift: age, structure, and history of the Tanzanian Craton. Geochimica et Cosmochimica Acta 63 (7–8), 1203–1217. http://dx.doi.org/10.1016/S0016-7037(99)00004-6.

Condomines, M., Gronvold, K., Hooker, P.J., Muehlenbachs, K., O'Nions, R.K., Oskarsson, N., Oxburch, E.R., 1983. Helium. oxygen, strontium and neodymium isotopic relationships in Icelandic volcanics. Earth and Planetary Science Letters 66, 125–137.

Darling, W.G., Griesshaber, E., Andrews, J.N., Armannsson, H., O'Nions, R.K., 1995. The origin of hydrothermal and other gases in the Kenya Rift Valley. Geochimica et Cosmochimica Acta 59, 2501–2512. http://dx.doi.org/10.1016/0016-7037(95)00145-X (358).

Dawson, J.B., 2008. The Gregory Rift Valley and Neogene-Recent volcanoes of Northern Tanzania. Geological Society, London, Memoirs 33, 102.

Day, J.M.D., Hilton, D.R., Pearson, D.G., MacPherson, C.G., Kjarsgaard, B.A., Janney, P.E., 2005. Absence of a high time integrated ^{3}He/(U+Th) source in the mantle beneath continents. Geology 33, 733–736.

de Moor, J.M., Fischer, T.P., Sharp, Z.D., Hilton, D.R., Barry, P.H., Mangasini, F., Ramirez, C., 2013. Gas chemistry and nitrogen isotope compositions of cold mantle gases from Rungwe Volcanic Province, southern Tanzania. Chemical Geology Special Issue - Frontiers in Gas Geochemistry 339, 30–42 (this issue).

Delalande, M., Bergonzini, L., Gherardi, F., Guidi, M., Andre, L., Abdallah, I., Williamson, D., 2011. Fluid geochemistry of natural manifestations from the Southern Poroto–Rungwe hydrothermal system (Tanzania): Preliminary conceptual model. Journal of Volcanology and Geothermal Research 199 (1–2), 127–141. http://dx.doi.org/10.1016/j.jvolgeores.2010.11.002.

Delvaux, D., Hanon, M., 1993. Neotectonics of the Mbeya area, SW Tanzania. Mus roy Afr centr, Tervuren. Dept. Geol. Min. Rapp. Ann, pp. 87–97.

Delvaux, D., Kraml, M., Sierralta, M., Wittenberg, A., Mayalla, J.W., Kabaka, K., Makene, C., GEOTHERM working group, 2010. Surface exploration of a viable geothermal resource in Mbeya area, SW Tanzania. Part I: Geology, Proceedings, World Geothermal Congress 2010, Bali, Indonesia 25– 29 April.

Ebinger, C.J., Furman, T., 2003. Geodynamical setting of the Virunga volcanic province, East Africa. Acta Vulcanologica 15 (1–2), 9–16.

Ebinger, C.J., Sleep, N.H., 1998. Cenozoinc magmatism through-out east Africa resulting from impact of a single plume. Nature 395, 788–791. http://dx.doi.org/10.1038/27417.

Ebinger, C.J., Rosendahl, B.R., Reynolds, D.J., 1987. Tectonic model of the Malawi rift, Africa. Tectonophysics 141, 215–235. http://dx.doi.org/10.1016/0040-1951(87)90187-9.

Ebinger, C.J., Bechtel, T.D., Forsyth, D.W., Bowin, C.O., 1989a. Effective elastic plate thickness beneath the East African and Afar Plateaus and dynamic compensation of the uplifts. Journal of Geophysical Research 94, 2883–2901. http://dx.doi.org/10.1029/JB094iB03p02883.

Ebinger, C.J., Deino, A.L., Drake, R.E., Tesha, A.L., 1989b. Chronology of volcanism and rift Basin propagation: Rungwe Volcanic Province, East Africa. Journal of Geophysical Research 94, 15,785–15,803. http://dx.doi.org/10.1029/B094iB11p15785.

Ebinger, C.J., Klerkx, J., Delvaux, D., Wuest, A., 1993. Evaluation of Natural Hazards in the Northern Part of the Malawi Rift (Tanzania). Mus. roy. Afr. centr., Tervuren (Belg.), Dept. Geol, Min., Rapp, ann. 1991–1992, pp. 83–86.

Ebinger, C., Djomani, Y., Mbede, Y., Foster, F., Dawson, J., 1997. Rifting Archean lithosphere: the Eyasi–Manyara–Natron rifts, East Africa. Journal of the Geological Society of London 154, 947–960.

Einarsson, P., 2008. Plate boundaries, rifts and transform zones in Iceland. Jökull 58, 35–58.

Elderfield, H., Schultz, A., 1996. Mid-ocean ridge hydrothermal fluxes and the chemical composition of the ocean. Annual Review of Earth and Planetary Sciences 24, 191–224.

Ellis, A.J., Golding, R.M., 1963. The solubility of carbon dioxide above 100 °C in water and sodium chloride solutions. American Journal of Science 261, 47–60.

Fischer, T.P., Burnard, P., Marty, B., Hilton, D.R., Füri, E., Palhol, F., Sharp, Z.D., Mangasini, F., 2009. Upper-mantle volatile chemistry at Oldoinyo Lengai volcano and the origin of carbonatites. Nature 459, 77–80. http://dx.doi.org/10.1038/nature07977.

Fontijn, K., Ernst, G.G.J., Elburg, M.A., Williamson, D., Abdallah, E., Kwelwa, S., Mbede, E., Jacobs, P., 2010a. Holocene explosive eruptions in the Rungwe Volcanic Province, Tanzania. Journal of Volcanology and Geothermal Research 196, 91–110.

Fontijn, K., Delvaux, D., Ernst, G.G.J., Kervyn, M., Mbede, E., Jacobs, P., 2010b. Tectonic control over active volcanism at a range of scales: case of the Rungwe Volcanic Province, SW Tanzania; and hazard implications. Journal of African Earth Sciences 58, 764–777.

Fontijn, K., Williamson, D., Mbede, E., Ernst, G., 2011. The Rungwe Volcanic Province, Tanzania – A volcanological review. Journal of African Earth Sciences 63 (2012), 12–31. http://dx.doi.org/10.1016/j.jafrearsci.2011.11.005.

Füri, E., Hilton, D.R., Halldorsson, S.A., Barry, P.H., Hahm, D., Fischer, T.P., Gronvold, K., 2010. Apparent decoupling of the He and Ne isotope systematics of the Icelandic mantle: the role of He depletion, melt mixing, degassing fractionation and air interaction. Geochimica et Cosmochimica Acta 74, 3307–3332. http://dx.doi.org/10.1016/j.gca.2010.03.023.

Furman, T., 1995. Melting of metasomatized subcontinental lithosphere: Undersaturated mafic lavas from Rungwe, Tanzania. Contributions to Mineralogy and Petrology 122, 97–115. http://dx.doi.org/10.1007/s004100050115.

Furman, T., 2007. Geochemistry of East African Rift basalts: an overview. Journal of African Earth Sciences 48 (2–3), 147–160. http://dx.doi.org/10.1016/j.jafrearsci.2006.06.00.

Furman, T., Bryce, J., Karson, J., Iotti, A., 2004. East African Rift System (EARS) plume structure: insights from Quaternary Mafic Lavas of Turkana, Kenya. Journal of Petrology 45, 1069–1088. http://dx.doi.org/10.1093/petrology/egh004.

Gautheron, C., Moreira, M., 2002. Helium signature of the subcontinental lithospheric mantle. Earth and Planetary Science Letters 199, 39–47. http://dx.doi.org/10.1016/S0012-821X(02)00563-0.

George, R., Rogers, N., Kelley, S., 1998. Earliest magmatism in Ethiopia: evidence for two mantle plumes in one flood basalt province. Geology 26, 923–926. http://dx.doi.org/10.1130/0091-7613(1998) 026<0923:EMIEEF>2.3.CO;2.

Giggenbach, W.F., Sano, Y., Wakita, H., 1993. Isotopes of He, and CO_2 and CH_4 contents in gases produced along the New Zealand part of a convergent plate boundary. Geochimica et Cosmochimica Acta 57, 3427–3455. http://dx.doi.org/10.1016/0016-7037(93)90549-C.

Graham, D.W., 2002. Noble gas isotope geochemistry of mid-ocean and ocean island basalts: characterization of mantle source reservoirs. Reviews in Mineralogy and Geochemistry 47, 247–317. http://dx.doi.org/10.2138/rmg.2002.47.8.

Hahm, D., Hilton, D.R., Cho, M., Wei, H., Kim, K.R., 2008. Geothermal He and CO_2 variations at Changbaishan intra-plate volcano (NE China) and the nature of the subcontinental lithospheric mantle. Geophysical Research Letters 33, L12304. http://dx.doi.org/10.1029/2008GL035955.

Harkin, D.A., 1955. The Sarabwe Lava Flow, Kiejo, Rungwe District. Tanganyika Notes 40, 20–23.

Harkin, D.A., 1960. The Rungwe Volcanics at the Northern End of Lake Nyasa, Geological Survey of Tanganyika, Dodoma. 172 pp.

Hilton, D.R., 1996. The helium and carbon isotope systematics of a continental geothermal system: results from monitoring studies at Long Valley caldera, California, U.S.A. Chemical Geology 127, 269–295. http://dx.doi.org/10.1016/0009-2541(95)00134-4.

Hilton, D.R., Gronvöld, K., O'Nions, R.K., Oxburgh, E.R., 1990. Regional distribution of ^{3}He anomalies in the Icelandic crust. Chemical Geology 88, 53–67.

Hilton, D.R., Hammerschmidt, K., Teufel, S., Friedrichsen, H., 1993. Helium isotope characteristics of Andean geothermal fluids and lavas. Earth and Planetary Science Letters 120, 265–282. http://dx.doi.org/10.1016/0012-821X(93)90244-4.

Hilton, D.R., Fischer, T.P., Marty, B., 2002. Noble gases and volatile recycling at subduction zones. Mineralogical Society Of America 47, 319–370. http://dx.doi.org/10.2138/rmg.2002.47.9.

Hilton, D.R., Halldórsson, S.A., Barry, P.H., Fischer, T.P., de Moor, J.M., Ramirez, C.J., Mangasini, F., Scarsi, P., 2011. Helium isotopes at Rungwe Volcanic Province, Tanzania, and the origin of East African Plateaux. Geophysical Research Letters 38, L21304. http://dx.doi.org/10.1029/2011GL049589.

Hochstein, M.P., Temu, E.P., Moshy, C.M.A., 2000. Geothermal resources of Tanzania Proceedings World Geothermal Congress. Kyushu–Tohoku, Japan, May 28 to June 10, 2000, pp. 1233–1238.

Hopp, J., Trieloff, M., Altherr, R., 2007. Noble gas compositions of the lithospheric mantle below the Chyulu Hills volcanic field, Kenya. Earth and Planetary Science Letters 261, 635–648. http://dx.doi.org/10.1016/j.epsl.2007.07.027.

Iranga, M.D., 1992. Seismicity of Tanzanian: distribution in time, space, magnitude, and strain release. Tectonophysics 209, 313–320.

James, T.C., 1967. Thermal springs in Tanzania. Transactions Applied Earth Science 76, B1–B18 (sect.B).

Kraml, M., Mnjokava, T.T., Mayalla, J.W., Kabaka, K., GEOTHERM working group, 2010. Surface exploration of a viable geothermal resource in Mbeya area, SW Tanzania - Part II: Geochemistry. Proceedings World Geothermal Congress 2010, Bali, Indonesia, pp. 25–29.

Kulongoski, J.T., Hilton, D.R., 2002. A quadrupole-based mass spectrometric system for the determination of noble gas abundances in fluids. Geochemistry, Geophysics, Geosystems 3, 1032–1042. http://dx.doi.org/10.1029/2001GC000267.

Lee, C.T., Rudnick, R.L., 1999. Compositionally stratified cratonic lithosphere: petrology and geochemistry of peridotite xenoliths from the Labait tuff cone, Tanzania. Proceedings of the Seventh International Kimberlite Conference, pp. 503–521.

Lupton, J.E., Baker, E.T., Massoth, G.J., 1989. Variable ^{3}He/heat ratios in submarine hydrothermal systems: evidence from two plumes over the Juan de Fuca Ridge. Nature 337, 161–164.

Maboko, M.A.H., 2000. Nd and Sr isotopic investigation of the Archean–Proterozoic boundary in north eastern Tanzania: constraints on the nature of Neoproterozoic tectonism in the Mozambique Belt. Precambrian Research 102 (1–2), 87–98. http://dx.doi.org/10.1016/S0301-9268(00)00060-7.

Manya, S., Kobayashi, K., Maboko, M.A.H., Nakamura, E., 2006. Ion microprobe zircon U–Pb dating of the late Archean metavolcanics and associated granites of the Musoma–Mara Greenstone Belt, Northeast Tanzania: implications for the geological evolution of the Tanzania Craton. Journal of African Earth Sciences 45 (3), 355–366. http://dx.doi.org/10.1016/j.jafearsci.2006.03.004.

Marty, B., Jambon, A., 1987. C/^{3}He in volatile fluxes from the solid Earth: implication for carbon geodynamics. Earth and Planetary Science Letters 83, 16–26. http://dx.doi.org/10.1016/0012-82X(87)90047-1.

Marty, B., Tolstikhin, I.N., 1998. CO_2 fluxes from mid-ocean ridges, arcs and plumes. Earth and Planetary Science Letters 145, 233–248. http://dx.doi.org/10.1016/S0009-2541(97)00145-9.

Marty, B., Jambon, A., Sano, Y., 1989. Helium isotopes and CO_2 in volcanic gases of Japan. Chemical Geology 76 (1989), 25–40. http://dx.doi.org/10.1016/0009-2541(89)90125-3.

Marty, B., Pik, R., Yirgu, G., 1996. Helium isotopic variations in Ethiopian plume lavas: nature of magmatic sources and limit on lower mantle contribution. Earth and Planetary Science Letters 144, 223–237. http://dx.doi.org/10.1016/0012-821X(96)00158-6.

McDougall, I., Kristjansson, L., Saemundsson, K., 1984. Magnetostratigraphy and geochronology of northwest Iceland. Journal of Geophysical Research 89, 7029–7060. http://dx.doi.org/10.1029/JB089iB08p07029.

Mnjokava, T.T., 2007. Interpretation of Exploration Geochemical Data for Geothermal Fluids from the Geothermal Field of the Rungwe Volcanic Area, SWTanzania. UNU-GTP Reykjavík, Iceland, Reports 2007, Number 14, pp. 303–332.

Mook, W.G., Bommerson, J.C., Stavermann, W.H., 1974. Carbon isotope fractionation between dissolved bicarbonate and gaseous carbon dioxide. Earth and Planetary Science Letters 22, 169. http://dx.doi.org/10.1016/0012-821X(74)90078-8.

Morrison, P., Pine, J., 1955. Radiogenic origin of the Helium isotopes in rock. Annals of the New York Academy of Sciences 62, 71–92. http://dx.doi.org/10.1111/j.1749-6632.1955.tb35366.x.

Mutlu, H., Güleç, N., Hilton, D.R., 2008. Helium–carbon relationships in geothermal fluids of western Anatolia, Turkey. Chemical Geology 247, 305–321. http://dx.doi.org/10.1016/j.chemgeo.2007.10.021.

Nyblade, A.A., et al., 2000. Seismic evidence for a deep upper mantle plume thermal anomaly beneath east Africa. Geology 28, 599–602. http://dx.doi.org/10.1130/0091-7613(2000) 28<599:SEFADU>2.0.CO;2.

O'Nions, R.K., Oxburgh, E.R., 1988. Helium, volatile fluxes and the development of continental crust. Earth and Planetary Science Letters 90 (1988), 331–347.

Ozima, M., Podosek, F.A., 1983. Noble Gas Geochemistry. Cambridge University Press, Cambridge, p. 367.

Park, Y., Nyblade, A., 2006. P-wave tomography reveals a westward dipping low velocity zone beneath the Kenya Rift. Geophysical Research Letters 33, 4. http://dx.doi.org/10.1029/2005GL025605.

Pik, R., Deniel, C., Coulon, C., Yirgu, G., Marty, B., 1999. Isotopic and trace element signatures of Ethiopian flood basalts: evidence for plume–lithosphere interactions. Geochimica et Cosmochimica Acta 63, 2263–2279. http://dx.doi.org/10.1016/S0016-7037(99)00141-6.

Pik, R., Marty, B., Hilton, D.R., 2006. How many mantle plumes in Africa? The geochemical point of view. Chemical Geology 226, 100–114. http://dx.doi.org/10.1016/j.chemgeo.2005.09.016.

Porcelli, D., Ballentine, C.J., 2002. An overview of noble gas geochemistry and cosmochemistry. In: Porcelli, D., Ballentine, C.J., Wieler, R. (Eds.), Noble Gases in Geochemistry and Cosmochemistry: Rev. Mineral. Geochem., vol. 47, pp. 1–19.

Poreda, R.J., Arnórsson, S., 1992. Helium isotopes in Icelandic geothermal systems: II. Helium–heat relationships. Geochimica et Cosmochimica Acta 56, 4229–4235.

Poreda, R.J., Craig, H., Arnórsson, S., Welhan, J.A., 1992. Helium isotopes in Icelandic geothermal systems: I., ^{3}He gas chemistry, and ^{13}C relations. Geochimica et Cosmochimica Acta 56, 4221–4228. http://dx.doi.org/10.1016/0016-7037(92)90263-I.

Ray, M.C., Hilton, D.R., Munoz, J., Fischer, T.P., Shaw, A.M., 2009. The effects of volatile recycling, degassing and crustal contamination on the helium and carbon geochemistry of hydrothermal fluids from the Southern Volcanic Zone of Chile. Chemical Geology 266 (1–2), 38–49. http://dx.doi.org/10.1016/j.chemgeo.2008.12.026.

Ritsema, J., Van Heijst, H., Woodhouse, J., 1999. Complex shear wave velocity structure imaged beneath Africa and Iceland. Science 286, 1925–1928. http://dx.doi.org/10.1126/science.286.5446.1925.

Rogers, N.W., 2006. Basaltic magmatism and the geodynamics of the East African Rift System. In: Yirgu, G., Ebinger, C.J., Maguire, P.K.H. (Eds.), The afar volcanic province within the East African Rift System: Geological Society Special Publication, 259, pp. 77–93. http://dx.doi.org/10.1144/GSL.SP.2006.259.01.08.

Rogers, N., McDonald, R., Fitton, J.G., George, R., Smith, M., Barreiro, B., 2000. Two mantle plumes beneath the East African rift system: Sr, Nd and Pb isotope evidence from Kenya Rift basalts. Earth and Planetary Science Letters 176, 387–400. http://dx.doi.org/10.1016/S0012-821X(00)00012-1.

Rudnicki, M.D., Elderfield, H., 1992. Theory applied to the Mid-Atlantic Ridge hydrothermal plumes: the finite difference approach. Journal of Volcanology and Geothermal Research 50, 163–174.

Sano, Y., Marty, B., 1995. Origin of carbon in fumarolic gas from island arcs. Chemical Geology 119, 265–274.

Sano, Y., Nakamura, Y., Wakita, H., Urabe, A., Tominaga, Y., 1984. ^{3}He emission related to volcanic activity. Science 224, 150–151. http://dx.doi.org/10.1126/science.224.4645.150.

Scarsi, P., Craig, H., 1996. Helium isotope ratios in Ethiopian Rift basalts. Earth and Planetary Science Letters 144, 505–516. http://dx.doi.org/10.1016/S0012-821X(96)00185-9.

Schilling, J.G., Kingsley, R.H., Hanan, B.B., McCully, B.L., 1992. Nd–Sr–Pb isotopic variations along the gulf of Aden: evidence for mantle plume–continental lithosphere interactions. Journal of Geophysical Research 97, 10927–10966. http://dx.doi.org/10.1029/92JB00415.

Shaw, A.M., Hilton, D.R., Fischer, T.P., Walker, J.A., Alvarado, G.E., 2003. Contrasting He-C relationships in Nicaragua and Costa Rica; insights into C cycling through subduction zones. Earth and Planetary Science Letters 214 (3–4), 499–513. http://dx.doi.org/10.1016/S0012-821X(03)00401-1.

Smets, B., Tedesco, D., Kervyn, F., Kies, A., Vaselli, O., Yalire, M.M., 2010. Dry gas vents ("mazuku") in Goma region (North-Kivu, Democratic Republic of Congo): Formation and risk assessment. Journal of African Earth Sciences 50, 787–798. http://dx.doi.org/10.1016/j.jafrearsci.2010.04.008.

Staples, R., White, R., Brandsdottir, B., Menke, W., Maguire, P., McBride, J., 1997. Faroes-Iceland experiment - 1: the crustal structure of northeastern Iceland. Journal of Geophysical Research 102, 7849–7866.

Stephen, H., Stephen, T., 1963. Solubilities of Inorganic and Organic Compounds, I. Binary Systems, Part I. Pergamon Press.

Stuart, F.M., Lass-Evand, S., Fitton, J.G., Ellam, R.M., 2003. High ^{3}He/^{4}He ratios in picritic basalts from Baffin Island and the role of a mixed reservoir in mantle plumes. Nature 424, 57–59. http://dx.doi.org/10.1038/nature01711.

Szaran, J., 1997. Achievement of carbon isotope equilibrium in the system HCO_3^- (solution)–CO_2 (gas). Chemical Geology 142, 79–86. http://dx.doi.org/10.1016/S0009-2541(97)00077-6.

Tedesco, D., Tassi, F., Vaselli, O., Poreda, R.J., Darrah, T., Cuoco, E., Yalire, M.M., 2010. Gas isotopic signatures (He, C, and Ar) in the Lake Kivu region (Western branch of the East Africa rift system): Geodynamic and volcanological implications. Journal of Geophysical Research 115 (B01205), 450. http://dx.doi.org/10.1029/2008JB006227.

Tiab, D., Donaldson, E.C., 2011. Petrophysics Theory and Practice of Measuring Reservoir Rock and Fluid Transport Properties. Gulf Publishing Company, Houston, TX. 53.

Torgersen, T., Jenkins, W.J., 1982. Helium isotopes in geothermal systems: Iceland, The Geysers, Raft River and Steamboat Springs. Geochimica et Cosmochimica Acta 46, 739–748. http://dx.doi.org/10.1016/0016-7037(82)90025-4.

Tuttle, M.L., Lockwood, J.P., Evans, W.C., 1990. Natural hazards associated with Lac Kivu and adjoining areas of the Virunga Volcanic Field, Rwanda and Zaïre, Central Africa: Final Report: USGS Open File Report, 90–691. 40pp.

Van Soest, M.C., Hilton, D.R., Kreulen, R., 1998. Tracing crustal and slab contributions to arc magmatism in the Lesser Antilles island arc using helium and carbon relationships in geothermal fluids. Geochimica et Cosmochimica Acta 62, 3323–3335. http://dx.doi.org/10.1016/S0016-7037(98)00241-5.

Vogel, J.C., Grootes, P.M., Mook, W.G., 1970. Isotope fractionation between gaseous and dissolved carbon dioxide. Zeitschrift für Physik 230, 255–258. http://dx.doi.org/10.1007/BF01394688.

Weiss, R.F., 1971. Solubility of Helium and Neon in Water and Seawater. Journal of Chemical and Engineering Data 16 (2), 235–241. http://dx.doi.org/10.1021/je60049a019.

Williams, T.M., Henney, P.J., Owen, R.B., 1993. Recent eruptive episodes of the Rungwe Volcanic Field (Tanzania) recorded in lacustrine sediments of the Northern Malawi Rift. Journal of African Earth Sciences 17, 33–39.

Yirgu, G., Ebinger, C.J., Maguire, P.K.H., 2006. The structure and evolution of the East African Rift System in the Afar Volcanic Province. Geological Society Special Publication 259, 1–327. http://dx.doi.org/10.1144/GSL.SP.2006.259.01.01.

Zhang, J., Quay, P.D., Wilbur, D.O., 1995. Carbon isotope fractionation during gas–water exchange and dissolution of CO_2. Geochimica et Cosmochimica Acta 59, 107–1146. http://dx.doi.org/10.1016/0016-7037(95)91550-D.